Cell

Circular RNA vaccines against SARS-CoV-2 and emerging variants

Graphical abstract

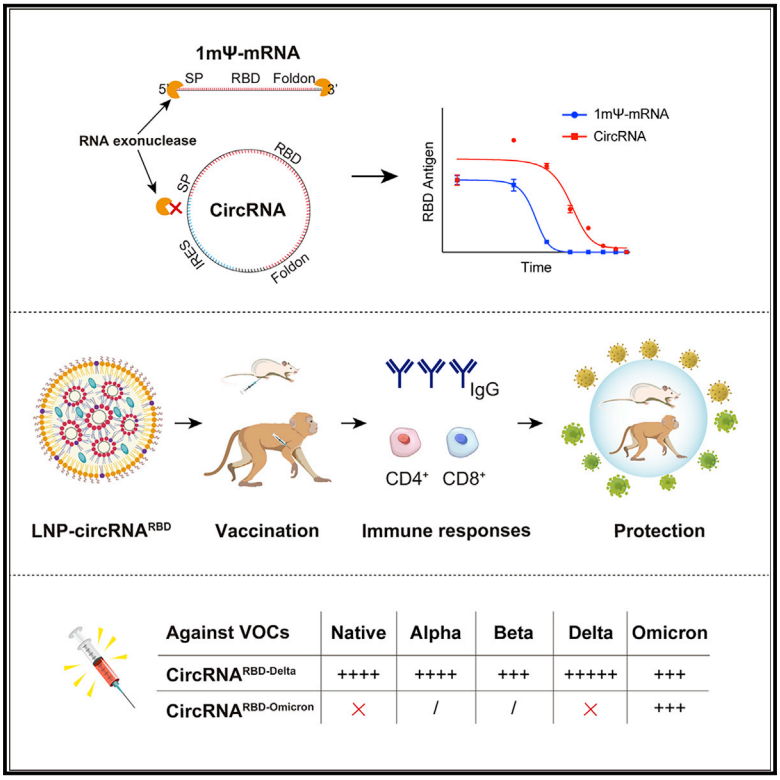

Authors

Liang Qu, Zongyi Yi, Yong Shen, ..., Jianwei Wang, Xiaoliang Sunney Xie, Wensheng Wei

Correspondence

wswei@pku.edu.cn

In brief

A circular RNA (circRNA) vaccine that encodes the trimeric RBD antigens of SARS-CoV-2 spike provides protection and memory boosting against SARS-CoV-2 variants of concern, in mice and rhesus macaques.

Highlights

- Highly stable circRNA vaccines induce potent humoral and cellular immune responses
- CircRNA vaccines elicit a high proportion of neutralizing antibodies
- CircRNA vaccines enable effective protection against SARS-CoV-2 in mice and monkeys
- CircRNA$^{RBD\text{-}Delta}$ vaccine provides broad-spectrum protection against SARS-CoV-2 VOCs

Qu et al., 2022, Cell *185*, 1728–1744
May 12, 2022
https://doi.org/10.1016/j.cell.2022.03.044

CellPress

CellPress
OPEN ACCESS

Cell

Article

Circular RNA vaccines against SARS-CoV-2 and emerging variants

Liang Qu,[1,9] Zongyi Yi,[1,2,9] Yong Shen,[1,2,9] Liangru Lin,[1] Feng Chen,[1,2] Yiyuan Xu,[1] Zeguang Wu,[1] Huixian Tang,[1] Xiaoxue Zhang,[1,2] Feng Tian,[1] Chunhui Wang,[1] Xia Xiao,[3,8] Xiaojing Dong,[3,8] Li Guo,[3,8] Shuaiyao Lu,[4] Chengyun Yang,[4] Cong Tang,[4] Yun Yang,[4] Wenhai Yu,[4] Junbin Wang,[4] Yanan Zhou,[4] Qing Huang,[4] Ayijiang Yisimayi,[5] Shuo Liu,[6] Weijin Huang,[6] Yunlong Cao,[5] Youchun Wang,[6] Zhuo Zhou,[1] Xiaozhong Peng,[4,7] Jianwei Wang,[3,8] Xiaoliang Sunney Xie,[5] and Wensheng Wei[1,10,*]

[1]Biomedical Pioneering Innovation Center, Beijing Advanced Innovation Center for Genomics, Peking-Tsinghua Center for Life Sciences, Peking University Genome Editing Research Center, State Key Laboratory of Protein and Plant Gene Research, School of Life Sciences, Peking University, Beijing 100871, China
[2]Academy for Advanced Interdisciplinary Studies, Peking University, Beijing 100871, China
[3]NHC Key Laboratory of Systems Biology of Pathogens and Christophe Mérieux Laboratory, Institute of Pathogen Biology, Chinese Academy of Medical Sciences and Peking Union Medical College, Beijing 100730, China
[4]National Kunming High-level Biosafety Primate Research Center, Institute of Medical Biology, Chinese Academy of Medical Sciences and Peking Union Medical College, Kunming, Yunnan, China
[5]Biomedical Pioneering Innovation Center, Beijing Advanced Innovation Center for Genomics, Peking-Tsinghua Center for Life Sciences, Peking University, Beijing 100871, China
[6]Division of HIV/AIDS and Sex-transmitted Virus Vaccines, Institute for Biological Product Control, National Institutes for Food and Drug Control (NIFDC) and WHO Collaborating Center for Standardization and Evaluation of Biologicals, Beijing 102629, China
[7]State Key Laboratory of Medical Molecular Biology, Department of Molecular Biology and Biochemistry, Institute of Basic Medical Sciences, Medical Primate Research Center, Neuroscience Center, Chinese Academy of Medical Sciences, School of Basic Medicine Peking Union Medical College, Beijing 100730, China
[8]Key Laboratory of Respiratory Disease Pathogenomics, Chinese Academy of Medical Sciences and Peking Union Medical College, Beijing 100730, China
[9]These authors contributed equally
[10]Lead contact
*Correspondence: wswei@pku.edu.cn
https://doi.org/10.1016/j.cell.2022.03.044

SUMMARY

As the emerging variants of SARS-CoV-2 continue to drive the worldwide pandemic, there is a constant demand for vaccines that offer more effective and broad-spectrum protection. Here, we report a circular RNA (circRNA) vaccine that elicited potent neutralizing antibodies and T cell responses by expressing the trimeric RBD of the spike protein, providing robust protection against SARS-CoV-2 in both mice and rhesus macaques. Notably, the circRNA vaccine enabled higher and more durable antigen production than the 1mΨ-modified mRNA vaccine and elicited a higher proportion of neutralizing antibodies and distinct Th1-skewed immune responses. Importantly, we found that the circRNA$^{RBD\text{-}Omicron}$ vaccine induced effective neutralizing antibodies against the Omicron but not the Delta variant. In contrast, the circRNA$^{RBD\text{-}Delta}$ vaccine protected against both Delta and Omicron or functioned as a booster after two doses of either native- or Delta-specific vaccination, making it a favorable choice against the current variants of concern (VOCs) of SARS-CoV-2.

INTRODUCTION

Coronavirus disease 2019 (COVID-19) is a serious worldwide public health emergency caused by a severe acute respiratory syndrome coronavirus (SARS-CoV-2) (Wu et al., 2020; Zhou et al., 2020). To date, COVID-19 has resulted in over 470 million confirmed cases and over 6 million confirmed deaths (World Health Organization). With the development of the epidemic, variants with immune escapability have appeared, the most serious of which is Omicron. By the end of January 2022, Omicron accounted for ~85% of COVID-19 cases (GISAID). Omicron carries over 30 mutations on the spike protein, 15 of which are located in the receptor-binding domain (RBD) (Dejnirattisai et al., 2022), resulting in a significant decrease in the effectiveness of prior neutralizing antibodies (Cameroni et al., 2022; Cao et al., 2021; Cele et al., 2022; Liu et al., 2022a; Planas et al., 2022). Although it has recently been reported that an additional boost with original SARS-CoV-2 vaccines after receiving a prior two-dose

vaccination regimen could partly elevate the neutralizing capability, the neutralization of Omicron pseudovirus was 4- to 13-fold lower than that of the wild type (Garcia-Beltran et al., 2022). This poses a severe challenge to the efficacy of current vaccines, highlighting the urgent need to develop effective vaccines against such fast-spreading variants.

SARS-CoV-2 belongs to the genus *Betacoronavirus* of the *Coronaviridae* family (V'Kovski et al., 2021). SARS-CoV-2 is a single-strand, positive-sense, enveloped virus, with an inner capsid formed by a 30-kb RNA genome wrapped by the nucleocapsid (N) proteins and a lipid envelope coated with the membrane (M), envelope (E), and spike (S) proteins (Kim et al., 2020). The S protein of SARS-CoV-2, composed of the S1 and S2 subunits, is the major surface protein of the virion. The S protein mediates viral entry into host cells by binding to its receptor, angiotensin-converting enzyme 2 (ACE2), through the RBD at the C terminus of the S1 subunit. This binding subsequently induces the fusion between the SARS-CoV-2 envelope and the host cell membrane mediated by the S2 subunit, which leads to the release of the viral genome into the cytoplasm (Hoffmann et al., 2020; Shang et al., 2020; Wrapp et al., 2020; Yan et al., 2020).

The S protein, S1 subunit, or RBD antigen of SARS-CoV-2 can induce both B cell and T cell responses, generating highly potent neutralizing antibodies against SARS-CoV-2 (Bangaru et al., 2020; Hsieh et al., 2020; Walls et al., 2020). Vaccination is the most promising approach to end the COVID-19 pandemic. Traditional vaccine platforms such as inactivated, virus-like particles and viral vector-based vaccines have been adopted to develop SARS-CoV-2 vaccines (Dai et al., 2020; Gao et al., 2020; Krammer, 2020; Mullard, 2020; Sanchez-Felipe et al., 2021; van Doremalen et al., 2020; Yang et al., 2020; Yu et al., 2020; Zhu et al., 2020). Importantly, mRNA vaccines against SARS-CoV-2 have been developed at warp speed and rapidly approved for use (Corbett et al., 2020a, 2020b; Huang et al., 2021; Laczkó et al., 2020; Sahin et al., 2020; Vogel et al., 2021; Zhang et al., 2020), even though the strategy was still in clinical trials and had never been applied commercially before (Pardi et al., 2018). The mRNA vaccine contains a linear single-stranded RNA consisting of a 5′ cap, the untranslated region (UTR), the antigen-coding region, and a 3′ polyA tail and is delivered into the body via lipid nanoparticle (LNP) encapsulation (Pardi et al., 2018). The clinical-scale mRNA vaccines could be manufactured rapidly upon the release of the viral antigen sequence (Corbett et al., 2020a). However, due to its susceptibility to exonuclease digestion, the current mRNA vaccine still has certain limitations including inherent instability and suboptimal thermostability after LNP encapsulation for *in vivo* administration (Durymanov and Reineke, 2018; Fenton et al., 2016; Jackson et al., 2020). Therefore, mRNA vaccine manufacturing necessitates an extremely sterile and strictly RNase-free environment during the whole production process, and its storage and distribution often requires low-temperature cold chain, limiting its availability in low-resource countries or regions (Uddin and Roni, 2021). Furthermore, because the mRNA produced by *in vitro* transcription (IVT) has a rather short half-life in cells, it requires additional nucleotide modifications (e.g., 1-methylpseudouridine) to improve its stability while reducing the risk of unwanted immunogenicity (Karikó et al., 2005; Pardi et al., 2018).

Unlike the linear conformation of mRNA, circular RNAs (circRNAs) are covalently closed ring RNA molecules that comprise a large class of noncoding RNAs generated in eukaryotic cells by a noncanonical RNA splicing event, called backsplicing(Chen, 2016; Kristensen et al., 2019; Zhang et al., 2014). Compared with the linear mRNA, circRNA is highly stable due to its covalently closed ring structure, which protects it from exonuclease-mediated degradation (Enuka et al., 2016; Kristensen et al., 2019; Memczak et al., 2013). It has been reported that circRNAs were more stable than their linear mRNA counterparts, with the circRNAs having the median half-life at least 2.5 times longer than their linear mRNA isoforms in mammalian cells (Enuka et al., 2016; Kristensen et al., 2019; Memczak et al., 2013). To date, only a few endogenous circRNAs have been shown to function as protein translation templates (Gao et al., 2021; Legnini et al., 2017; Zhang et al., 2018a; Zhang et al., 2018b). Although circRNA lacks the essential elements for cap-dependent translation, it can be engineered to enable protein translation through an internal ribosome entry site (IRES) or the incorporation of the m6A modification upstream of the open reading frame (ORF) (Wesselhoeft et al., 2018; Yang et al., 2017). Thus, we envisioned that circRNA could be leveraged as a platform to generate immunogens.

Although the potential immunogenicity of IVT-produced circRNA has been the source of much debate (Chen et al., 2019; Liu et al., 2022b; Wesselhoeft et al., 2019), it is tempting to test whether circRNA could be developed into a safe and effective vaccine platform. Given the inherent stability and an avoidable need for nucleotide modifications, we attempted to develop circRNA vaccines, aiming to provide effective protection against SARS-CoV-2 and its emerging variants.

RESULTS

CircRNA^{RBD} produced functional SARS-CoV-2 RBD antigens

We employed the group I intron autocatalysis strategy (Wesselhoeft et al., 2018) to produce circRNAs encoding SARS-CoV-2 RBD antigens, termed circRNA^{RBD} (Figure 1A). In this construct, the IRES element was placed before the RBD-coding sequence to initiate its translation. To enhance the immunogenicity of RBD antigens, the signal peptide sequence of human tissue plasminogen activator (tPA) was fused to the N terminus of RBD to ensure the secretion of antigens (Kou et al., 2017; Pardi et al., 2017; Richner et al., 2017). In addition, recent research reported that spike trimers outperformed monomeric spikes in binding human ACE2 (hACE2) (Bouwman et al., 2021; Wrapp et al., 2020; Yan et al., 2020). To improve the immunogenicity of RBD antigens, the trimerization motif of bacteriophage T4 fibritin protein (foldon) (Papanikolopoulou et al., 2008) was fused to its C terminus. This IRES-SP-RBD-foldon sequence was then cloned into the vector to construct the IVT template for producing circRNA^{RBD} (Figure 1A; Table S1).

To produce high-purity circRNA^{RBD}, we first optimized the IVT reaction to generate circRNA^{RBD} (Figure S1A) without the extra step of GTP catalysis (Wesselhoeft et al., 2018). High-performance liquid chromatography (HPLC) analysis

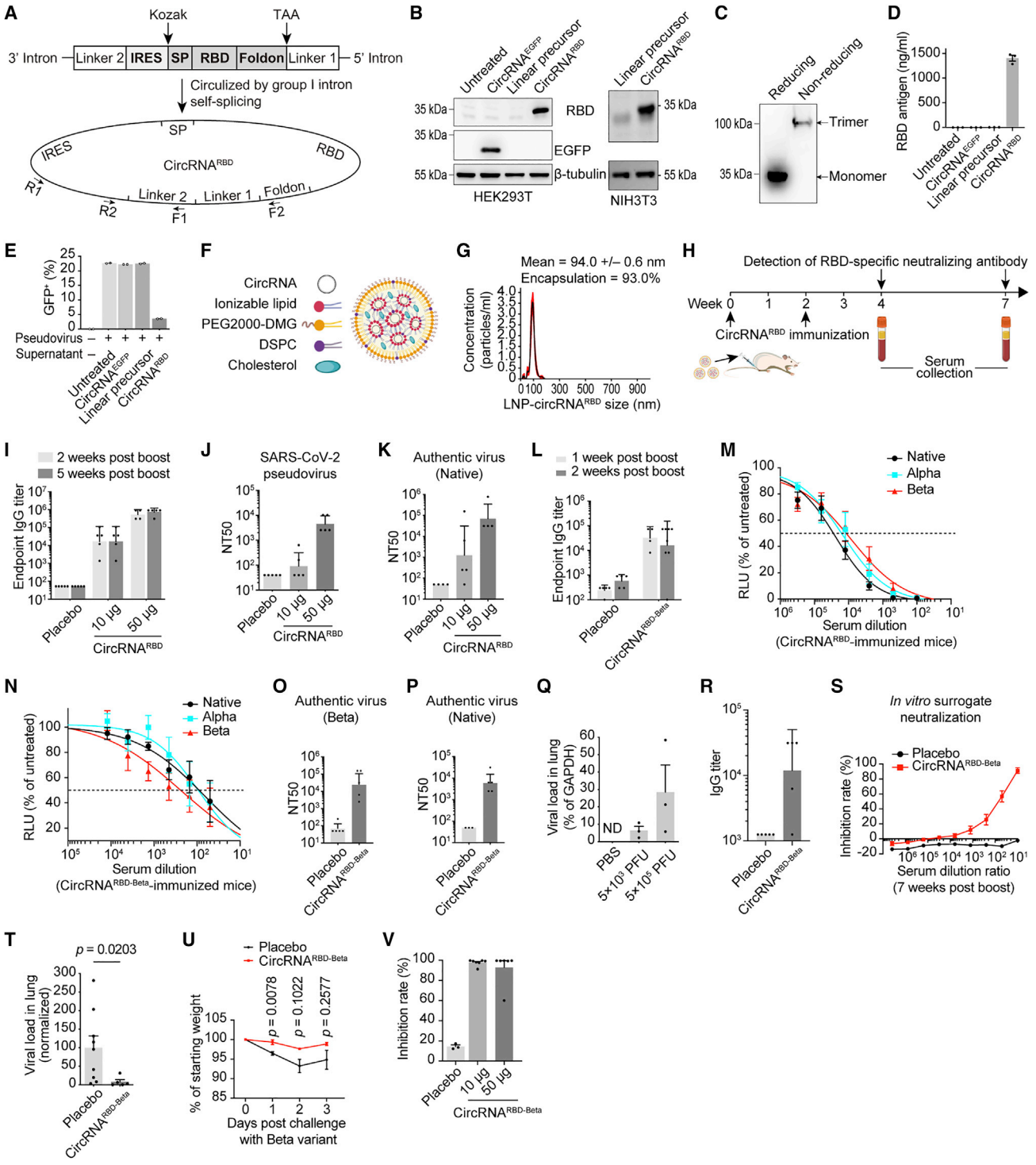

Figure 1. Immunogenicity and protection of circRNA vaccines against SARS-CoV-2 in mice

(A) Schematic diagram of circRNA^{RBD} circularization by group I intron autocatalysis. SP, signal peptide sequence of human tPA. Foldon, the trimerization domain from bacteriophage T4 fibritin. The arrows indicate the design of primers for PCR analysis.

(B) Western blot showing the expression level of RBD in the supernatant of HEK293T or NIH3T3 cells transfected with circRNA^{RBD}. The circRNA^{EGFP} and linear RNA precursor were used as controls.

(C) Western blot result under reducing conditions (with DTT) or nonreducing conditions (without DTT).

(D) Measurement of the concentration of RBD in the supernatant of HEK293T cells by ELISA.

(legend continued on next page)

determined that the latter half of the main peak contained high-purity circRNA (Figures S1B and S1C). Then we successfully manufactured circRNA^{RBD} in large quantities (Figures S1D and S1E). We found that the majority of the purified circRNA^{RBD} fractions were resistant to exonuclease-RNase R, whereas the nicked RNA^{RBD} were almost completely degraded, indicating that purified circRNA^{RBD} were mostly in circular format (Figure S1F). The purity of circRNA^{RBD} was over 90%, calculated via the denaturing gel electrophoresis and the subsequent semi-quantitative analysis (Figures S1G–S1I). The circularization of circRNA^{RBD} was further verified by reverse transcription-PCR, Sanger sequencing, and RNase H-mediated specific cleavage (Figures S1J–S1M).

To test the secretory expression of RBD produced by circRNA^{RBD}, the purified circRNA^{RBD} was transfected into HEK293T cells or NIH3T3 cells. Abundant RBD antigens in the supernatant of both human and murine cells were detected by western blot, indicating the high compatibility of circRNAs (Figure 1B). With the help of foldon, the circRNA^{RBD} encoded stable homogeneous RBD trimers in the supernatant, which were dissociated into monomers under reducing conditions (Figure 1C). The concentration of RBD antigens produced by circRNA^{RBD} reached ~1,400 ng/mL, 600-fold higher than those produced by its linear precursor RNA (Figure 1D).

In addition to the group I intron-based strategy, we also developed a T4 RNA ligase-based method to produce circRNAs. This method adopted the complementary pairing sequence of split IRES as the splint instead of a DNA splint to generate an intramolecular RNA nick structure serving as the catalytic substrate of T4 RNA ligase (Figure S2A; Table S2). Sanger sequencing confirmed the precise circularization of circRNA^{RBD} by this approach (Figure S2B). Similarly, abundant RBD antigens were detected in the supernatant at a concentration of ~1,000 ng/mL, which was ~200-fold higher than those produced by its linear precursor RNA (Figures S2C and S2D).

To verify whether the secreted SARS-CoV-2 RBD antigens produced by circRNA^{RBD} were functional, the supernatants of circRNA^{RBD}-transfected cells were used in a competition assay using hACE2-overexpressing HEK293 cells (HEK293T-ACE2) and SARS-CoV-2 pseudovirus harboring an enhanced green fluorescent protein (EGFP) reporter (Ou et al., 2020). The secreted RBD antigens could effectively block SARS-CoV-2 pseudovirus infection (Figure 1E).

SARS-CoV-2 circRNA^{RBD} vaccine induced sustained humoral immune responses with high levels of neutralizing antibodies

To explore whether circRNA could be leveraged to create a vaccine, we attempted to assess the immunogenicity of circRNA^{RBD} encapsulated with LNP in BALB/c mice (Figure 1F). The circRNA^{RBD} encapsulation efficiency was greater than 93%, with an average diameter of 100 nm (Figure 1G). Mice were immunized through intramuscular (i.m.) injection with 10 or 50 μg of LNP-circRNA^{RBD} vaccines twice at a 2-week interval (Figure 1H). The circRNA^{RBD} elicited a high level of RBD-specific IgG endpoint geometric mean titers (GMTs), reaching ~1.9×10^4 for the 10-μg dose and ~5.7×10^5 for the 50-μg dose (Figure 1I).

Sera from circRNA^{RBD}-vaccinated mice effectively neutralized SARS-CoV-2 pseudovirus with a 50% neutralization titer (NT50) of ~4.5×10^3 (Figure 1J) and authentic SARS-CoV-2 virus with an NT50 of ~7.0×10^4 (Figure 1K).

SARS-CoV-2 circRNA$^{RBD\text{-}Beta}$ vaccine-elicited antibodies showed preferential neutralizing activity against the Beta variant

Next, we evaluated the efficacy of circRNA$^{RBD\text{-}Beta}$, a circRNA vaccine encoding RBD/K417N-E484K-N501Y antigens derived from the SARS-CoV-2 Beta variant. Mice were immunized with LNP-circRNA$^{RBD\text{-}Beta}$ through i.m. injection twice at a 2-week interval. The immunized mice's sera were collected at 1 and 2 weeks

(E) Competitive inhibition assay of SARS-CoV-2 pseudovirus infection by the circRNA^{RBD}-translated RBD antigens.
(F) Schematic representation of the LNP-circRNA complex.
(G) Representative intensity-size graph of LNP-circRNA^{RBD} by the dynamic light scattering method.
(H) Schematic diagram of the circRNA^{RBD} vaccination and antibody analysis in BALB/c mice.
(I) Measurement of the IgG antibody endpoint GMTs elicited by the circRNA^{RBD} vaccine.
(J) Measurement of the NT50 of LNP-circRNA^{RBD}-immunized mouse sera using pseudoviruses.
(K) Neutralization assay of SARS-CoV-2 authentic virus with the sera of mice immunized with circRNA^{RBD} vaccine. The serum samples were collected at 5 weeks after the boost.
(L) Measurement of the SARS-CoV-2 (Beta) specific IgG endpoint GMTs elicited by the circRNA$^{RBD\text{-}Beta}$ vaccine.
(M and N) Sigmoidal curve diagram of the neutralization of vesicular stomatitis virus (VSV)-based D614G, Alpha, or Beta pseudovirus with the sera of mice immunized with circRNA^{RBD} (M) or circRNA$^{RBD\text{-}Beta}$ (N). The sera were collected 1 week after the boost.
(O and P) Neutralization assay of SARS-CoV-2 Beta (O) or D614G (P) authentic virus with the serum of mice immunized with circRNA$^{RBD\text{-}Beta}$ vaccine.
(Q) Measurement of the viral loads in the mouse lung tissues. The SARS-CoV-2 RNA copies were normalized to *GAPDH*.
(R) Measurement of the SARS-CoV-2 RBD-Beta-specific IgG endpoint GMTs.
(S) Sigmoidal curve diagram of the inhibition rate by sera from immunized mice with surrogate virus neutralization assay. In (R) and (S), the sera were collected 3 days before challenge.
(T) Viral loads in the lung tissues of challenged mice.
(U) The weight change of immunized or placebo mice after challenge.
(V) Measurement of the neutralizing activity of sera from mice immunized with circRNA$^{RBD\text{-}Beta}$ vaccine. The circRNAs were encapsulated with LNPs (Precision Nanosystems) instead of the lab-prepared LNPs.
In (D) and (E), data are shown as the mean ± SEM (n = 2 or 3). In (I)–(L), (O), (P), and (R), data are shown as the geometric mean ± geometric SD (n = 3–6). In (M), (N), (Q), and (S)–(V), data are shown as the mean ± SEM (n = 3–7). Each symbol represents an individual mouse. Unpaired two-sided Student's t test was performed for comparison, as indicated.
See also Figures S1 and S2.

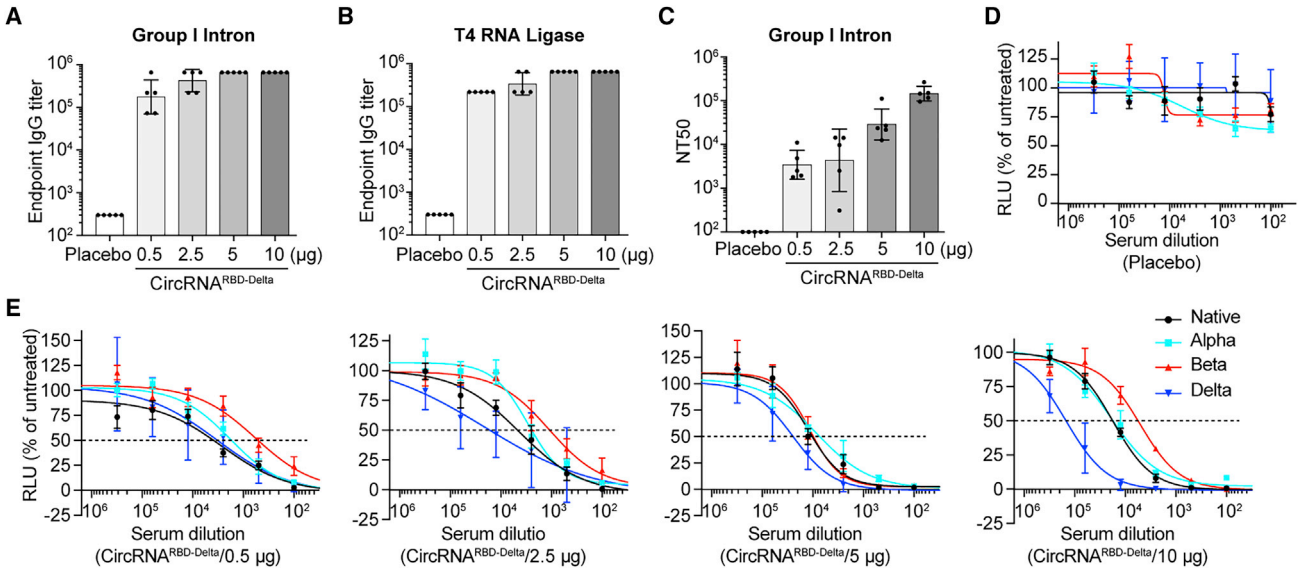

Figure 2. Humoral immune responses elicited by circRNA$^{RBD\text{-}Delta}$ vaccines in mice

(A) Measurement of the SARS-CoV-2 Delta-specific IgG endpoint GMTs elicited by circRNA$^{RBD\text{-}Delta}$ vaccine generated by group I intron.

(B) Measurement of the SARS-CoV-2 Delta-specific IgG endpoint GMTs elicited by circRNA$^{RBD\text{-}Delta}$ vaccine generated by T4 RNA ligases.

(C) Neutralization assay of VSV-based SARS-CoV-2 (Delta) pseudovirus with the sera of mice immunized with circRNA$^{RBD\text{-}Delta}$ vaccines.

(D and E) Sigmoidal curve diagram of the neutralization assay.

In (A)–(C), data are shown as the geometric mean ± geometric SD (n = 5), and each symbol represents an individual mouse. In (D) and (E), data are shown as the mean ± SEM (n = 5).

after the boost. ELISA showed that the RBD-Beta-specific IgG endpoint GMT was ~1.6 × 10^4 at 1 week after the boost (Figure 1L). Pseudovirus neutralization assays revealed that circRNA^{RBD}-elicited antibodies could effectively neutralize all three pseudoviruses, with the highest neutralizing activity against the native (D614G) strain (Figure 1M). The circRNA$^{RBD\text{-}Beta}$-elicited antibodies could also neutralize all three pseudoviruses, with the highest activity against its corresponding Beta variant (Figure 1N).

In line with pseudovirus neutralization assay, the sera from immunized mice neutralized the authentic SARS-CoV-2 Beta and native (D614G) strains with NT50 values of 2.6 × 10^4 (Figure 1O) and 6.0 × 10^3 (Figure 1P), respectively.

CircRNA$^{RBD\text{-}Beta}$ vaccine protected mice against infection with the Beta variant

To further evaluate the protective efficacy of circRNA$^{RBD\text{-}Beta}$ vaccine, we employed the authentic Beta variant for challenge experiments. Consistent with a recent report (Gu et al., 2020; Chen et al., 2021; Montagutelli et al., 2021), the Beta variant could infect wild-type BALB/c mice and replicate in their lungs (Figure 1Q), likely due to mutations in the spike such as K417N, E484K, and N501Y. Notably, 7 weeks after the boost dose, the RBD-Beta-specific IgG endpoint GMT was still approximately 1.2 × 10^4 (Figure 1R), with significant neutralizing activity against RBD-Beta antigens (Figure 1S). Each immunized mouse was then intranasally infected with 5 × 10^4 plaque forming unit (PFU) of Beta virus (7 weeks post-boost). Lung tissues were collected 3 days after the challenge for the detection of viral RNAs. The viral loads in the lungs of circRNA-vaccinated mice were significantly lower than those of the placebo group (Figure 1T). Consistently, only the mice in the placebo group exhibited weight loss (Figure 1U). These results indicated that the circRNA$^{RBD\text{-}Beta}$ vaccine could effectively protect the mice against SARS-CoV-2 Beta.

Considering that a high dose of circRNA^{RBD} was necessary to elicit maximal level of neutralizing antibodies, we postulated that the LNP delivery platform might have a great impact on the efficacy of the circRNA vaccine. After multiple tests, we were able to significantly lower the vaccine dose using one of the commercial formulas (Precision Nanosystems). In this regard, 10 μg of circRNA could induce neutralizing antibodies at a comparable level to 50 μg (Figure 1V). We thus switched our choice of LNP for the rest of our experiments.

CircRNA$^{RBD\text{-}Delta}$ vaccine induced potent neutralizing antibodies against SARS-CoV-2 Delta

The Delta variant, like the Beta variant, partially escapes the antibodies produced in survivors or vaccinees (Lustig et al., 2021; Planas et al., 2021; Torgovnick, 2021). To develop such a variant-specific vaccine, we adopted both group I intron and T4 RNA ligase ligation strategies to produce circRNA$^{RBD\text{-}Delta}$. Mice were immunized i.m. with 0.5, 2.5, 5, or 10 μg of circRNA$^{RBD\text{-}Delta}$ vaccines twice at a 2-week interval. Then, 2 weeks after the boost dose, the sera from immunized mice were collected to detect RBD-Delta-specific antibodies. Vaccines of circRNA$^{RBD\text{-}Delta}$ made by either circularization method could induce high endpoint GMTs (Figures 2A and 2B). The sera from circRNA$^{RBD\text{-}Delta}$-vaccinated mice effectively neutralized the Delta pseudovirus in a dose-dependent manner, with an NT50 of ~1.4 × 10^5 for the 10-μg dose (Figure 2C).

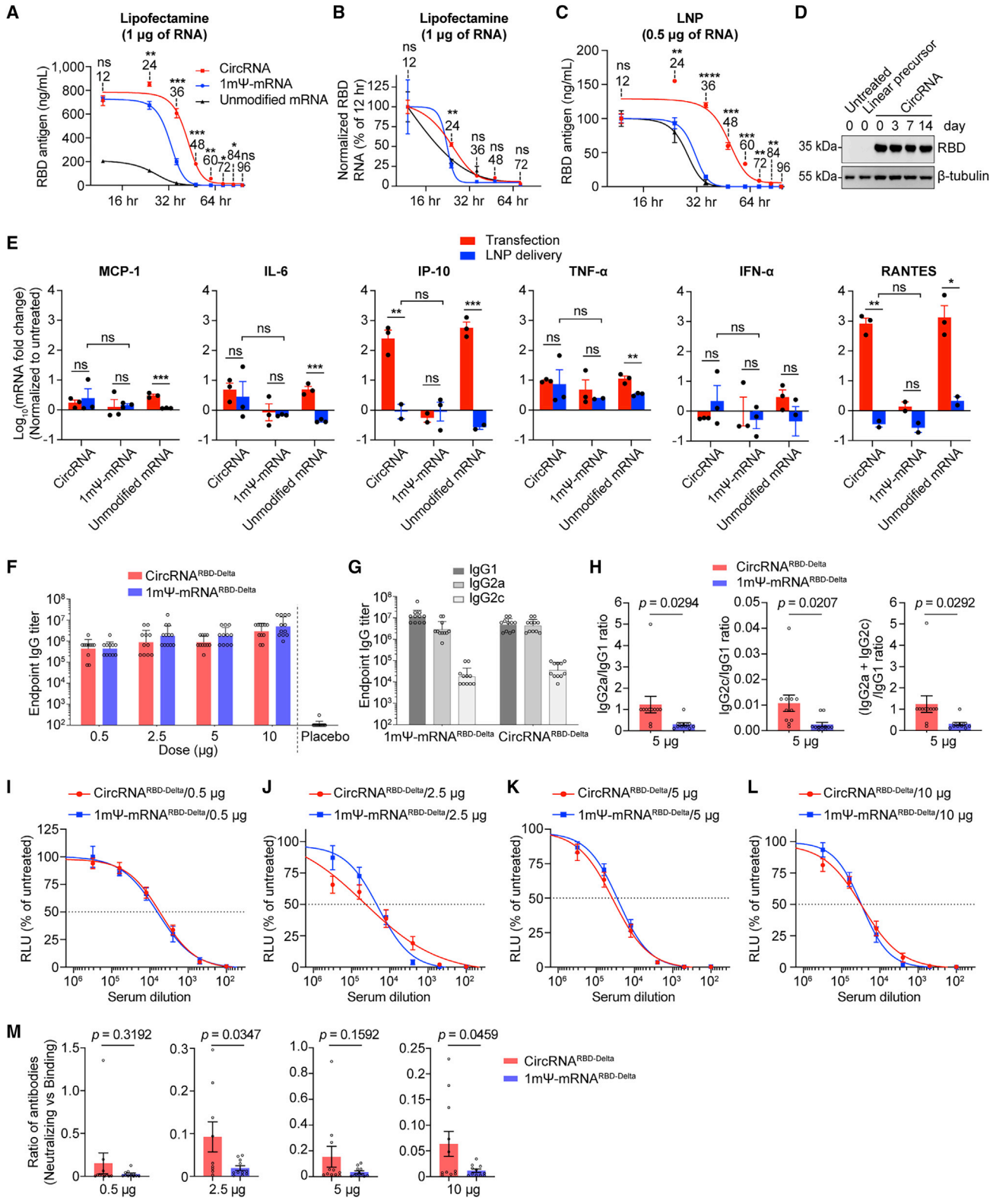

(legend on next page)

Importantly, circRNA$^{RBD\text{-}Delta}$ vaccines could provide protection against other variants, including the native strain, Alpha and Beta, albeit to varying degrees. The sera from circRNA$^{RBD\text{-}Delta}$-immunized mice exhibited the highest neutralizing activity against Delta and the lowest against Beta (Figures 2D and 2E).

CircRNA vaccine enabled higher and more durable antigen expression than mRNA vaccine

CircRNAs are reportedly more stable than mRNAs owing to their covalent closed circular structure (Fischer and Leung, 2017). To test whether the stability of the circRNA vaccine could confer higher and more durable antigen-encoding efficiency than the mRNA vaccine, we generated 1mΨ-modified mRNA (1mΨ-mRNA), and unmodified mRNA, both of which contained the same RBD-encoding sequence as the circRNA for a fair comparison (Figure S3A; Table S3). The circRNA produced much higher levels of RBD antigens at all time points than both 1mΨ-mRNA and unmodified mRNA, and they were maintained for a longer period (Figure 3A). RT-qPCR showed that circRNAs were more stable than mRNAs, modified or unmodified (Figure 3B). Importantly, LNP encapsulation further enhanced the advantage of circRNA in protein production and durability from both 1mΨ-mRNA and unmodified mRNA (Figure 3C). Interestingly, LNP encapsulation appeared to improve the antigen-encoding efficiency of unmodified mRNA to a level comparable with that of 1mΨ-mRNA (Figure 3C).

We found that even after 2 weeks of storage at room temperature (~25°C), the circRNA could express RBD antigens without detectable loss (Figure 3D), highlighting its remarkable thermal stability. To further evaluate the thermostability of the vaccines, the LNP-encapsulated circRNA, 1mΨ-mRNA, and unmodified mRNA were stored at 4°C, ~25°C, or 37°C for up to 28 days prior to transfection. At all temperatures tested, circRNA expressed higher levels of antigens than those of the other two mRNA groups (Figures S3B–S3D). At 4°C, little reduction in RBD antigens produced by LNP-circRNA could be detected from 1 to 28 days (Figure S3B). The stability of LNP-circRNA, 1mΨ-mRNA, or unmodified mRNA was clearly reduced with increasing storage temperature, especially at 37°C (Figures S3C and S3D).

Importantly, we found that the innate immune responses elicited by LNP-encapsulated circRNA^{RBD} were comparable with those by LNP-encapsulated 1mΨ-mRNA^{RBD} and significantly lower than those by the transfected RNAs (Figure 3E).

CircRNA vaccine elicited higher surrogate IgG ratios of Th1-biased responses and elevated proportions of neutralizing antibodies than mRNA vaccine

Given that circRNA vaccines possess higher stability and antigen-encoding efficiency, we wondered whether they exhibited distinctive immunogenicity, compared with mRNA vaccines. We compared the balance of Th1/Th2 immune responses between circRNA$^{RBD\text{-}Delta}$ and mRNA$^{RBD\text{-}Delta}$ vaccines, because Th2-biased immune responses might induce vaccine-associated enhanced respiratory disease (VAERD) (Corbett et al., 2020a; Graham, 2020; Sahin et al., 2020). ELISA showed that the total IgG elicited by circRNA$^{RBD\text{-}Delta}$ was comparable with that by 1mΨ-mRNA$^{RBD\text{-}Delta}$ (Figure 3F); however, the ratios of IgG2a/IgG1, IgG2c/IgG1, or (IgG2a + IgG2c)/IgG1 from circRNA$^{RBD\text{-}Delta}$ were consistently higher than those from 1mΨ-mRNA$^{RBD\text{-}Delta}$ vaccine (Figures 3G, 3H, S3E, and S3F), and this Th1-skewed T cell immune response was believed beneficial for the clearance of SARS-CoV-2 (Corbett et al., 2020a; Graham, 2020; Sahin et al., 2020).

Antibody-dependent enhancement (ADE) of infection by virus-specific antibodies is another potential concern for vaccines that has been reported for infections by some viruses, including Zika, Dengue, and coronaviruses (Dowd and Pierson, 2011; Halstead and O'Rourke, 1977; Rey et al., 2018; Takano et al., 2019; Wen et al., 2020). Previous research has reported that virus-binding antibodies without neutralizing activity elicited by infection or vaccination possibly caused ADE effects, especially for those viruses with different serotypes (Dejnirattisai et al., 2010; Martínez-

Figure 3. CircRNA vaccine elicited higher average proportions of neutralizing antibodies and distinct Th1-biased T cell immune responses than mRNA vaccine

(A) Comparison of the antigen expression levels of circRNA$^{RBD\text{-}Delta}$, 1mΨ-mRNA$^{RBD\text{-}Delta}$, and unmodified mRNA$^{RBD\text{-}Delta}$ through Lipofectamine MessengerMax transfection in HEK293T cells.

(B) The dynamic change in RNA levels in (A).

(C) The antigen expression levels of LNP-circRNA$^{RBD\text{-}Delta}$, LNP-1mΨ-mRNA$^{RBD\text{-}Delta}$, and LNP-unmodified-mRNA$^{RBD\text{-}Delta}$ in HEK293T cells. In (A)–(C), data are shown as the mean ± SEM (n = 3).

(D) Western blot showing the expression level of RBD in the supernatant of HEK293T cells transfected with circRNA^{RBD}.

(E) The mRNA abundance of cytokines (MCP-1, IL-6, IP-10, TNF-α, IFN-α, and RANTES) induced by circRNA$^{RBD\text{-}Delta}$, 1mΨ-mRNA$^{RBD\text{-}Delta}$, and unmodified mRNA$^{RBD\text{-}Delta}$ via RT-qPCR analysis in HEK293T cells. The circRNA, 1mΨ-mRNA, or unmodified mRNA was delivered into HEK293T cells via MessengerMax or LNP. The mRNA levels were normalized by *GAPDH*. The mRNA fold changes were normalized using the untreated HEK293T cells. Data are shown as the mean ± SEM (n = 2 or 3).

(F) Measurement of the RBD-Delta-specific IgG endpoint GMTs in mice.

(G) Measurement of RBD-Delta-specific IgG1/IgG2a/IgG2c endpoint GMTs in mice. In (F) and (G), data are shown as the geometric mean ± geometric SD (n = 11–12).

(H) Measurement of the specific IgG2a/IgG1, IgG2c/IgG1, and (IgG2a + IgG2c)/IgG1 ratios.

(I–L) Sigmoidal curve diagram of neutralization rate of VSV-based SARS-CoV-2 (Delta) pseudovirus with the sera from mice immunized with 0.5 μg (I), 2.5 μg (J), 5 μg (K), or 10 μg (L) of circRNA or 1mΨ-mRNA vaccines.

(M) The ratio of (neutralizing Ab)/(binding Ab) elicited by 0.5, 2.5, 5, or 10 μg of the circRNA or 1mΨ-mRNA vaccine. The ratio of (NT50)/(endpoint GMT) of each mouse was calculated. In (H)–(M), data are shown as the mean ± SEM (n = 10–12).

Unpaired two-sided Student's t test was performed for comparison, as indicated in the figures, *p < 0.05; **p < 0.01; ***p < 0.001; ****p < 0.0001; ns, not significant. Each symbol represents an individual mouse.

See also Figure S3.

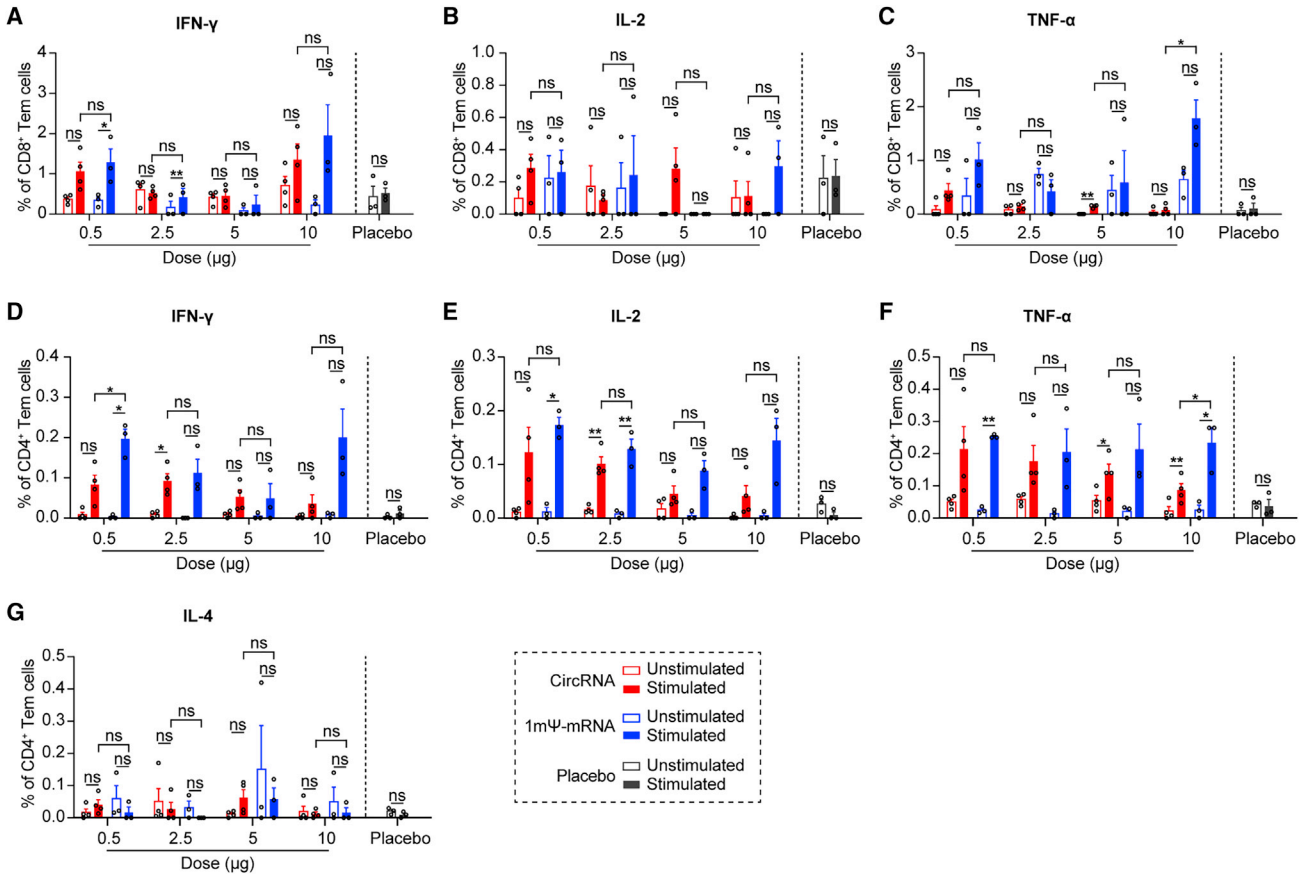

Figure 4. T cell immune responses elicited by SARS-CoV-2 circRNA$^{RBD\text{-}Delta}$ or mRNA$^{RBD\text{-}Delta}$ vaccines in mice

(A–C) FACS analysis results showing the percentages of CD8$^+$ Tem cells secreting IFN-γ (A), IL-2 (B), or TNF-α (C) after stimulation with RBD-Delta peptide pools. (D–G) FACS analysis results showing the percentages of CD4$^+$ Tem cells secreting IFN-γ (D), IL-2 (E), TNF-α (F), or IL-4 (G) after stimulation. Empty LNP was used as the control. In (A)–(G), data are presented as the mean ± SEM (n = 3 or 4), and each symbol represents an individual mouse.

Paired Student's t test was performed for comparison between the peptide pool-stimulated group and un-stimulated group as indicated; unpaired two-sided Student's t test was performed for comparison between circRNA$^{RBD\text{-}Delta}$ vaccines and mRNA$^{RBD\text{-}Delta}$ vaccines as indicated; *p < 0.05; **p < 0.01; ***p < 0.001; ****p < 0.0001; ns, not significant.

See also Figures S4 and S5.

Vega et al., 2017). Therefore, we compared the ratios of neutralizing to binding antibodies between circRNA and 1mΨ-mRNA vaccines. Although circRNA$^{RBD\text{-}Delta}$ exhibited equal neutralizing capability to 1mΨ-mRNA$^{RBD\text{-}Delta}$ (Figures 3I–3L), the former induced higher proportions of neutralizing antibodies at both 2.5- and 10-μg doses in mice (Figure 3M). Owing to this unique feature, the circRNA vaccine might have a certain advantage in circumventing potential ADE effects caused by viruses such as Dengue and Zika and better tolerating frequent viral mutations.

CircRNA$^{RBD\text{-}Delta}$ vaccine elicited SARS-CoV-2-specific T cell immune responses

B cells, CD4$^+$ T cells, and CD8$^+$ T cells mediated effector functions against SARS-CoV-2 in COVID-19 patients (Sette and Crotty, 2021). To compare CD4$^+$ and CD8$^+$ T cell immune responses, the splenocytes of immunized mice were collected and stimulated with SARS-CoV-2 RBD-Delta pooled peptides (Table S4), and cytokine-producing T cells were quantified by intracellular cytokine staining among effector memory T cells (Tem, CD44$^+$CD62L$^-$) (Figure S4). After stimulation with peptides, CD8$^+$ T cells producing IFN-γ, TNF-α, and IL-2 were detected in mice immunized with the circRNA$^{RBD\text{-}Delta}$ vaccine or 1mΨ-mRNA$^{RBD\text{-}Delta}$ vaccine (Figures 4A–4C), indicating the RBD-specific CD8$^+$ T cell responses elicited by both vaccines. The CD4$^+$ T cells of immunized mice induced strong IFN-γ, TNF-α, and IL-2 responses but minimal IL-4 responses (Figures 4D–4G). Consistent with the above results (Figures 3G, 3H, S3E, and S3F), these indicated that circRNA vaccines induced Th1-biased T cell immune responses (Figures 4D–4G and S5A–S5D).

CircRNA$^{RBD\text{-}Delta}$ vaccine elicited high levels of broad-spectrum neutralizing antibodies against both the Delta and Omicron variants

To cope with the current Omicron emergency, we tested the neutralizing capability elicited by all three circRNA vaccines against the Omicron variant. The neutralizing activity against Omicron elicited by each one of the three circRNA vaccines dropped

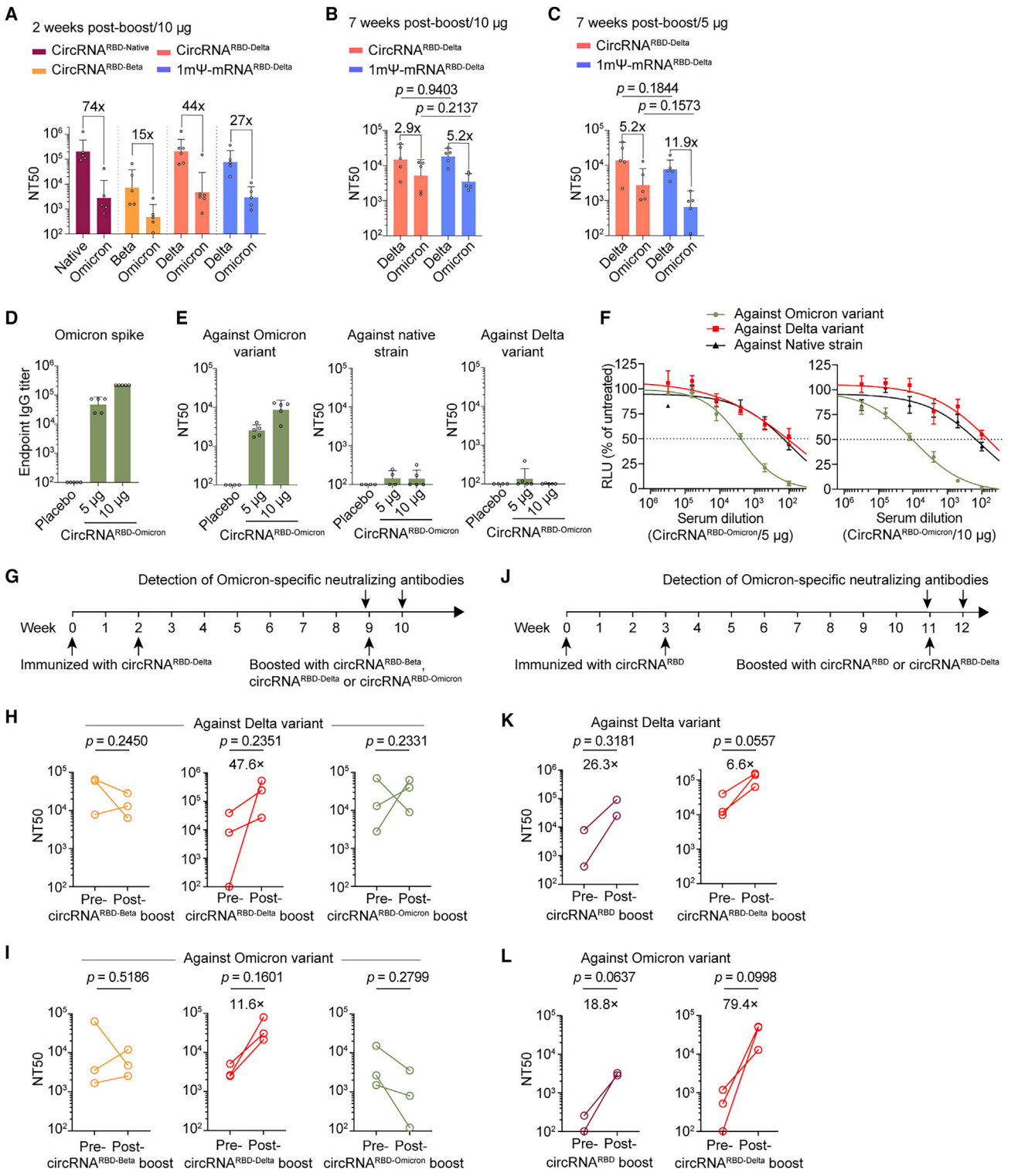

Figure 5. CircRNA$^{RBD\text{-}Delta}$ vaccine elicited high levels of neutralizing antibodies against both the Delta and Omicron variants

(A) Neutralization assay of VSV-based SARS-CoV-2 pseudovirus with the sera of immunized mice.

(B and C) Neutralization assay of VSV-based SARS-CoV-2 pseudovirus with the sera of mice immunized with 10 μg (B) or 5 μg (C) of circRNA or mRNA vaccines.

(D) Measuring the Omicron-spike-specific IgG endpoint GMTs of circRNA$^{RBD\text{-}Omicron}$-immunized mouse sera.

(legend continued on next page)

74-fold (native), 15-fold (Beta), and 44-fold (Delta) in comparison with the neutralizing activity against their corresponding variants (Figure 5A). Among all three, the circRNA$^{RBD\text{-}Delta}$ vaccine maintained sufficient neutralizing activity against Omicron (Figure 5A), with an NT50 of ~4.7 × 10^3, whereas the NT50 of the circRNA$^{RBD\text{-}Beta}$ against Omicron dropped below 5 × 10^2 (Figure 5A). Compared with the mRNA$^{RBD\text{-}Delta}$ vaccine, the circRNA$^{RBD\text{-}Delta}$ vaccine elicited comparable neutralizing activity against both Delta and Omicron variants for mouse sera collected 2 weeks after the boost (short-term) and 7 weeks after the boost (long-term) (Figures 5A–5C). Similar to the above observations (Figure 3M), the circRNA$^{RBD\text{-}Delta}$ vaccine also elicited a higher average proportion of neutralizing antibodies against Omicron variant than the 1mΨ-mRNA$^{RBD\text{-}Delta}$ vaccine at both 2 weeks after the boost (short-term) and 7 weeks after the boost (long-term) (Figures S6A–S6D), indicating the potential superiority of the circRNA vaccine against the circulating variants of SARS-CoV-2.

CircRNA$^{RBD\text{-}Omicron}$ vaccine elicited neutralizing antibodies against Omicron

We developed an Omicron-specific circRNA vaccine that expressed the trimeric RBD antigens of the Omicron variant. Mice were immunized i.m. with 5 or 10 μg of circRNA$^{RBD\text{-}Omicron}$ vaccines twice at a 2-week interval. Then,1 week after the boost dose, the serum samples from immunized mice were collected for the detection of specific antibodies. The circRNA$^{RBD\text{-}Omicron}$ vaccine induced Omicron spike-specific antibodies with the endpoint GMTs of ~4.7 × 10^4 for the 5-μg dose and ~2.2 × 10^5 for the 10-μg dose (Figure 5D), yielding clear neutralizing activities against Omicron with NT50 values of ~2.5 × 10^3 for the 5-μg dose and ~8.6 × 10^3 for the 10-μg dose (Figure 5E). However, neutralizing activity could hardly be detected against the native strain or Delta variant (Figures 5E and 5F).

The third booster with the circRNA$^{RBD\text{-}Delta}$ vaccine markedly elevated the neutralizing antibodies against the current VOCs

We next investigated the feasibility of circRNA vaccines as a booster. Mice immunized with two doses of circRNA$^{RBD\text{-}Delta}$ vaccines received a 3rd booster with circRNA$^{RBD\text{-}Beta}$, circRNA$^{RBD\text{-}Delta}$, or circRNA$^{RBD\text{-}Omicron}$ vaccine at 7 weeks after the 2nd dose, followed by the assessment of neutralizing activity at 1 week after boost (Figure 5G). Only circRNA$^{RBD\text{-}Delta}$ effectively boosted the neutralizing antibodies against both Delta (Figure 5H) and Omicron (Figure 5I). By contrast, the 3rd boost with the circRNA$^{RBD\text{-}Beta}$ or circRNA$^{RBD\text{-}Omicron}$ vaccine failed to elevate the neutralizing capability against Delta or Omicron (Figures 5H and 5I).

We then tested the 3rd booster with circRNA^{RBD} or circRNA$^{RBD\text{-}Delta}$ vaccine in mice previously immunized with two-dose circRNA^{RBD} vaccines (Figure 5J). Both vaccines effectively boosted neutralizing antibodies against both Delta (Figure 5K) and Omicron (Figure 5L). CircRNA$^{RBD\text{-}Delta}$ appeared to be a much better booster than circRNA^{RBD} against both Delta and Omicron variants, which elevated the geometric mean NT50 from ~4 × 10^2 to ~3.2 × 10^4 against the Omicron (Figures 5K and 5L).

Taken together, these results suggest that circRNA$^{RBD\text{-}Delta}$ might be a favorable choice for vaccination to provide broad-spectrum protection against the current VOCs.

CircRNA vaccine elicited potent neutralizing antibodies and Th1-biased immune responses in rhesus macaques

To further assess the immunogenicity of circRNA vaccine in nonhuman primates (NHPs), groups of 2- to 4-year-old rhesus macaques were immunized i.m. with 20, 100, or 500 μg of circRNA^{RBD} vaccines, 100 μg of circRNA^{Ctrl}, or PBS control on days 0 and 21 (Figure 6A). The specific antibodies were measured using the rhesus macaque plasma collected at 2 weeks after the boost (Figure 6A). The IgG endpoint GMTs reached ~2.1 × 10^4 (20-μg dose), ~1.6 × 10^4 (100-μg dose), and ~7 × 10^3 (500-μg dose) for circRNA^{RBD} vaccines, whereas circRNA^{Ctrl}- or PBS-immunized rhesus macaques failed to induce RBD-specific antibodies (Figure 6B). The pseudovirus neutralization assay showed NT50 values of ~180 for the 20-μg dose, ~520 for the 100-μg dose, and ~390 for the 500-μg dose (Figure 6C). The authentic SARS-CoV-2 neutralization assay showed NT50 values of ~80 for the 20-μg dose, ~120 for the 100-μg dose, and ~50 for the 500-μg dose (Figures 6D and 6E).

We then performed a cross-neutralizing assay. Both the pseudotyped and authentic SARS-CoV-2 neutralization assays showed that the circRNA^{RBD} vaccine-immunized rhesus macaque plasma could effectively inhibit the corresponding native strain, whereas the Alpha, Delta, and Beta variants could also be inhibited, but with reduced activity, especially against the Beta variant (Figures 6D and 6E).

Peripheral blood mononuclear cells (PBMCs) were collected on the day before challenge with SARS-CoV-2. The RBD-specific T cell responses in rhesus macaques were measured using PBMCs stimulated with the RBD peptide pools (Table S5). The

(E) Measurement of the NT50 of LNP-circRNA$^{RBD\text{-}Omicron}$-immunized mouse sera using VSV-based pseudoviruses. The serum samples were collected at 1 week after the boost dose. In (A)–(E), data are shown as the geometric mean ± geometric SD (n = 4 or 5).
(F) Sigmoidal curve diagram of the neutralization assay in (E). Data are shown as the mean ± SEM (n = 4 or 5).
(G) Schematic diagram of the circRNA boost and antibody detection in mice receiving two-dose prior circRNA$^{RBD\text{-}Delta}$ vaccine.
(H and I) Measurement of the NT50 value of mouse sera boosted with circRNA vaccine (5 μg) after receiving two-dose circRNA$^{RBD\text{-}Delta}$ vaccine (5 μg) using VSV-based pseudoviruses of Delta (H) or Omicron (I).
(J) Schematic diagram of the circRNA vaccination and antibody detection in mice receiving two-dose circRNA^{RBD} vaccine.
(K and L) Measurement of the NT50 value of mouse sera boosted with circRNA vaccine (20 μg) after receiving two-dose circRNA^{RBD} vaccine (20 μg) using VSV-based pseudoviruses of Delta (K) or Omicron (L).
In (B) and (C), unpaired two-sided Student's t test was performed for comparison, as indicated. In (H), (I), (K), and (L), paired Student's t test was performed for comparison, as indicated. Each symbol represents an individual mouse.
See also Figure S6.

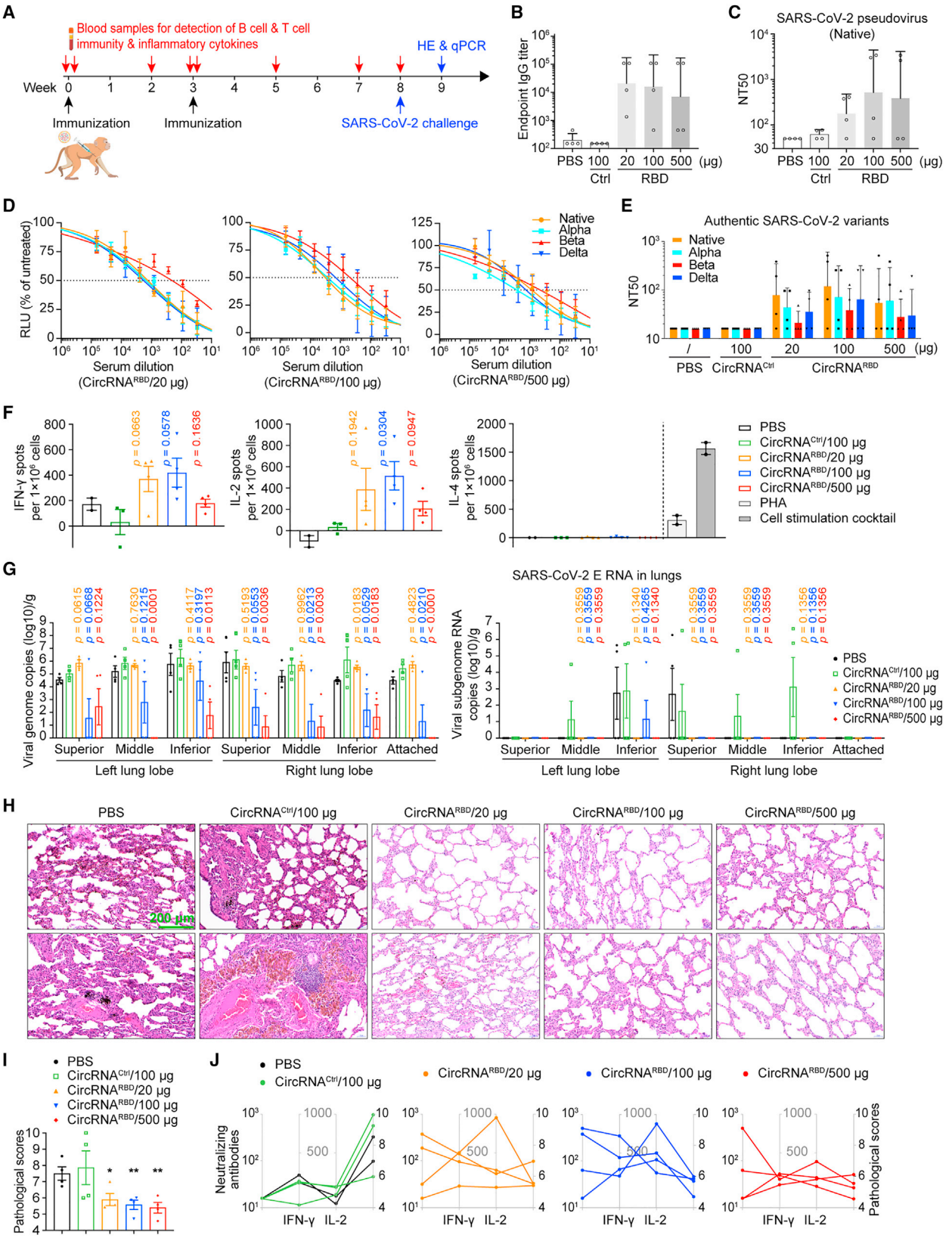

(legend on next page)

ELISpot assay showed evident IFN-γ and IL-2 responses but nearly undetectable IL-4 in circRNA^{RBD}-immunized rhesus macaques (Figure 6F), indicating a Th1-biased T cell immune response.

CircRNA vaccine protected the rhesus macaques against SARS-CoV-2 infection

Next, 5 weeks after the boost dose, the immunized rhesus macaques were challenged with 1 × 10^6 PFU of the SARS-CoV-2 native strain as described previously (Vogel et al., 2021). The challenged rhesus macaques were euthanized at 7 days post-infection (dpi), and the lung tissues underwent viral load and histopathological assays. The RT-qPCR assay, using primers targeting SARS-CoV-2 genomic RNA (N gene), indicated that the rhesus macaques immunized with 100 or 500 μg of circRNA^{RBD} vaccine were well protected as the viral genomic RNAs were reduced nearly 1,000-fold, compared with the control groups (Figure 6G). To detect the actively replicative viral loads, we performed qPCR using primers targeting SARS-CoV-2 subgenomic RNA (E gene) and found that rhesus macaques immunized with circRNA^{RBD} at all three doses had nearly no detectable viral subgenomic RNA in the lung tissues (Figure 6G).

Further histopathological examination demonstrated that circRNA^{RBD}-immunized rhesus macaques of all doses were well protected because only very mild pneumonia was observed (Figure 6H). By contrast, severe pneumonia was observed in the lungs of the two control groups, as exemplified by local pulmonary septal thickening, moderate hemorrhage in the pulmonary septals, a large number of scattered dust cells, and massive inflammatory cell infiltration (Figure 6H). The pathological scores further confirmed that circRNA^{RBD} immunization significantly protected the rhesus macaques against COVID-19 (Figure 6I), likely resulting from a synergy between the humoral immune responses and T cell responses by vaccination (Figure 6J).

CircRNA vaccine did not cause clinical signs of illness in rhesus macaques

To further evaluate the safety of circRNA vaccines in NHPs, physiological and biochemical indicators were monitored. No severe clinical adverse effects were observed following the priming or boost dose. CircRNA^{RBD} vaccines induced evident IL-6 and monocyte chemoattractant protein-1 (MCP-1) (Figures S7A and S7B), whereas TNF-α, IL-1β, and IFN-α were nearly undetectable (Figures S7C–S7E). The body temperatures of both immunized rhesus macaques and controls were within the normal range after prime and boost (Figure S7F). None of the challenged macaques showed clinical signs of illness (Figures S7G–S7K). Collectively, our study provides preliminary proof of safety for the circRNA vaccination in NHPs.

Expression of SARS-CoV-2 neutralizing antibodies via the circRNA platform

In addition to vaccines, circRNAs could be repurposed for therapeutics when used to express other proteins, antibodies, or peptides. Here, we attempted to test the therapeutic potential of circRNAs by expressing antibodies. It has been reported that SARS-CoV-2 neutralizing nanobodies or hACE2 decoys can inhibit SARS-CoV-2 infection (Linsky et al., 2020; Schoof et al., 2020; Xiang et al., 2020; Chan et al., 2020). This prompted us to leverage the circRNA platform to express SARS-CoV-2 neutralizing nanobodies and hACE2 decoys (Figure 7A). Pseudovirus neutralization assays showed that supernatants of HEK293T cells transfected with circRNA^{nAB} or circRNA$^{hACE2\ decoys}$ could effectively inhibit SARS-CoV-2 pseudovirus infection (Figure 7B).

Next, we tested neutralizing antibodies against the SARS-CoV-2 variants, Alpha and Beta. The supernatants of circRNA$^{nAB1\text{-}Tri}$ and circRNA$^{nAB3\text{-}Tri}$ effectively blocked Alpha and D614G pseudovirus infection (Figure 7C). However, both nanobodies showed markedly decreased neutralizing activity

Figure 6. CircRNA vaccine elicits immunogenicity and protection against SARS-CoV-2 infection in rhesus macaques

(A) Schematic diagram of the circRNA^{RBD} vaccination in rhesus macaques.

(B) Measurement of the SARS-CoV-2 RBD-specific IgG endpoint GMTs of the plasma from the rhesus macaques immunized with circRNA^{RBD} vaccine, or circRNA^{Ctrl} (circRNA without the RBD-encoding sequence), or PBS control.

(C) Measurement of the NT50 of the plasma of immunized rhesus macaques.

(D) Sigmoidal curve diagram of neutralization rate of VSV-based SARS-CoV-2 native, Alpha, Beta, and Delta pseudoviruses using the plasma of immunized rhesus macaques.

(E) Neutralization assay of authentic SARS-CoV-2 native, Alpha, Beta, and Delta viruses using the plasma of immunized rhesus macaques.

(F) ELISpot assay measurement of the SARS-CoV-2 RBD-specific IFN-γ, IL-2, and IL-4 responses of PBMCs from rhesus macaques immunized with circRNA vaccines. Data are shown as the mean ± SEM ($n \geq 2$).

(G) Measurement of the viral loads (N gene) and subgenome RNA loads (E gene) in the lung tissues of challenged rhesus macaques. Data are shown as the mean ± SEM ($n = 4$).

(H) H&E staining of pathological sections using the lung tissues from immunized rhesus macaques at 7 days after challenge.

(I) Pathological score of pneumonia based on the lung tissues from immunized rhesus macaques at 7 days after challenge. The data are shown as the mean ± SEM ($n = 4$).

(J) Correlation of the B cell response, T cell response, and pathological score in each immunized rhesus macaque. Each symbol represents an individual macaque and symbol of the same rhesus macaque is connected by line. B cell responses are shown by neutralizing antibody production as a value of NT50 against authentic SARS-CoV-2 virus. T cell responses are shown as spots per 10^6 PBMCs detected in an IFN-γ and IL-2 ELISpot assay. Pathological scores are the same as in (I).

In (B), (C) and (E), data are shown as the geometric mean ± geometric SD ($n = 4$). In (D), (F), (G), and (I), data are shown as the mean ± SEM ($n = 2$–4). Unpaired two-sided Student's t test was performed for comparison, as indicated in the figures; *$p < 0.05$; **$p < 0.01$; ***$p < 0.001$; ****$p < 0.0001$; ns, not significant. Each symbol represents an individual rhesus macaque.

See also Figure S7.

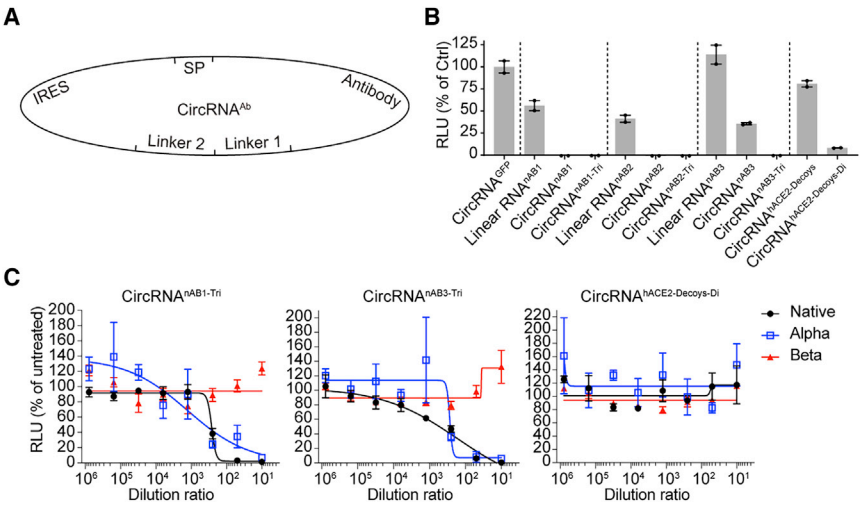

Figure 7. Expression of SARS-CoV-2 neutralizing nanobodies or hACE2 decoys via a circRNA platform

(A) Schematic diagram of circRNA^{nAB} or circRNA$^{hACE2\ decoys}$ circularization by group I intron.

(B) Lentivirus-based pseudovirus neutralization assay with the supernatant from cells transfected with circRNA encoding nAB1, nAB1-Tri, nAB2, nAB2-Tri, nAB3, and nAB3-Tri or ACE2 decoys. The nAB1-Tri, nAB2-Tri, and nAB3-Tri represent the trimers of nAB1, nAB2, and nAB3, respectively. The luciferase value was normalized to that of the circRNA^{EGFP} control.

(C) Sigmoidal curve diagram of neutralization of VSV-based SARS-CoV-2 D614G, Alpha, or Beta pseudovirus using the supernatant of cells transfected with nAB1-Tri, nAB3-Tri, or ACE2 decoys encoded by the corresponding circRNAs.

Data are shown as the mean ± SEM (n = 2 or 3).

against Beta variant (Figure 7C). The hACE2 decoys showed no inhibition activity against Alpha and Beta variants (Figure 7C).

DISCUSSION

COVID-19 is still a fast-growing global health crisis with circulating SAS-CoV-2 variants evading immunity from prior vaccination or viral infection, especially with the emerging Delta and Omicron VOCs (Karim and Karim, 2021; Muik et al., 2021; Wang et al., 2021a, 2021b). Our study established a circRNA vaccination strategy to elicit effective neutralizing antibodies and T cell immune responses against SARS-CoV-2 and its emerging variants.

As reported, most effective neutralizing antibodies recognize the RBD region of the spike protein (Barnes et al., 2020; Cao et al., 2020; Du et al., 2020; Koenig et al., 2021; Schoof et al., 2020; Xiang et al., 2020), and targeting the RBD may induce fewer non-neutralizing antibodies (Huang et al., 2021; Laczkó et al., 2020; Sahin et al., 2020; Tai et al., 2020; Zhang et al., 2020). Given that RBD trimers bind to hACE2 better than their monomeric counterparts and have been shown to enhance the humoral immune response (Bouwman et al., 2021; Routhu et al., 2021; Sahin et al., 2020), we chose to express RBD trimers via circRNA as the immunogen. The circRNA-encoded RBD trimers were functional and successfully induced potent neutralizing antibodies and specific T cell responses against SARS-CoV-2 in both mice and rhesus macaques (Figures 2, 4, and 6).

mRNA vaccines based on the full-length spike protein (mRNA-1273 and BNT162b2) (Corbett et al., 2020a, 2020b; Vogel et al., 2021) or RBD elicit neutralizing antibodies and T cell responses (Huang et al., 2021; Laczkó et al., 2020; Sahin et al., 2020; Tai et al., 2020; Zhang et al., 2020). In comparison with the mRNA vaccine, the circRNA vaccine elicited higher and more durable immunogens, leading to distinct Th1-biased T cell immune responses from the mRNA vaccine (Figures 3 and S3). Moreover, the circRNA$^{RBD\text{-}Delta}$ vaccine induced a higher average proportion of neutralizing antibodies against both Delta and Omicron variants than the mRNA$^{RBD\text{-}Delta}$ vaccine (Figures 3M and S6). We infer that the more durable antigen production and distinct immunogenicity of circRNA vaccine (Figures 3A–3E) enable the elicitation of a higher proportion of neutralizing antibodies and distinct Th1-skewed immune responses than the 1mΨ-modified mRNA vaccine (Figures 3G–3M), by promoting and elongating the antibody affinity maturation process in germinal centers after vaccination (Alameh et al., 2021; Liu et al., 2021).

A recent preprint reported that vaccinees who received two doses of SARS-CoV-2 vaccine exhibited enhanced neutralizing antibodies against Delta variant after infection with Omicron, implying that an Omicron vaccine might provide broad-spectrum protection against other variants (Khan et al., 2021). Our result argues against this possibility because our Omicron-specific vaccine failed to cross-protect against the Delta variant (Figures 5D–5F) or boost the two-dose Delta vaccine (Figures 5H and 5I). By contrast, the circRNA$^{RBD\text{-}Delta}$ vaccine appeared to produce antigens possessing high immunogenicity and consequently elicit a high level of neutralizing antibodies against Delta (Figures 2 and 3). Our Delta-specific vaccination could cross-protect against all other variants, including Omicron (Figures 2E, 5A, 5B, and 5C), and could also be used as an effective booster following two-dose original SARS-CoV-2 vaccines (Figures 5K and 5L). It is hoped that further testing will show that the circRNA$^{RBD\text{-}Delta}$ vaccine could be applied as an effective booster for current major vaccines.

Currently, mRNA-1273 and BNT162b2 were widely administrated, both of which were produced with complete replacement of uridine by 1-methylpseudouridine to reduce unwanted immunogenicity (Corbett et al., 2020a, 2020b; Karikó et al., 2005; Vogel et al., 2021). In this study, no nucleotide modification was used for the circRNA vaccine. We found that the immunogenicity of LNP-encapsulated circRNA^{RBD} was at a comparable level with that of LNP-encapsulated 1mΨ-mRNA^{RBD} in the cell culture (Figure 3E). Moreover, although our study was not specifically designed for studying the safety of vaccines or drugs, it is worth noting that circRNA vaccine did not cause clinical signs of illness or enhanced pathology in vaccinated NHPs, thereby opening avenues for the development of circRNA-based vaccines or drugs

(Figures 6 and S7). It will be interesting to see if nucleotide modifications can further improve the therapeutic applicability of circRNAs in future studies, given that it is currently technically challenging because the 1mΨ modification would disrupt IRES function (Wesselhoeft et al., 2019).

In this study, we also tested the therapeutic potential of circRNAs that encode SARS-CoV-2-specific neutralizing nanobodies (Barnes et al., 2020; Cao et al., 2020; Du et al., 2020; Koenig et al., 2021; Schoof et al., 2020; Xiang et al., 2020) or hACE2 decoys (Chan et al., 2020; Glasgow et al., 2020), which could effectively neutralize the SARS-CoV-2 pseudovirus (Figure 7). Beyond viral receptors, this circRNA expression platform holds the potential to become a therapeutic drug encoding therapeutic antibodies *in vivo*, such as anti-PD1/PD-L1 antibodies (Boutros et al., 2016; He and Xu, 2020). Unlike antibodies and protein drugs, circRNAs encode therapeutic antibodies in the cytoplasm, allowing them to target intracellular targets such as TP53 (Sabapathy and Lane, 2018) and KRAS (Mukhopadhyay et al., 2021), bypassing the cytomembrane barrier.

In summary, circRNA holds the potential to become an effective and safe platform for vaccination against viral infection—including SARS-CoV-2 emerging variants—as well as possibly becoming a therapeutic platform, owing to its specific properties.

Limitations of the study

The small numbers of rhesus macaques we used for the challenge experiments led to high variations and large error bars in the evaluation of circRNA vaccines. The immunogenicity of IVT-produced circRNAs is another potential concern (Chen et al., 2019; Liu et al., 2022b; Wesselhoeft et al., 2019). Even though our study showed that circRNA vaccines did not cause any clinical signs of illness in rhesus macaques, even at high doses (500 μg per rhesus macaque) (Figure 6), the safety of circRNA vaccines awaits further investigation in NHPs and clinical trials. In the current study, we observed that the circRNA vaccine outperformed its mRNA vaccine counterpart in several aspects; however, more detailed and comprehensive comparisons need to be conducted in the future. It is worth noting that the mRNA vaccine we used for the comparison study is different from the two widely administered vaccines, mRNA-1273 and BNT162b2, both of which encode the full-length spike antigens and were produced by different manufacturing processes, whereas the mRNA vaccine in this study encoded the trimeric RBD of spike (Corbett et al., 2020a, 2020b; Vogel et al., 2021).

STAR★METHODS

Detailed methods are provided in the online version of this paper and include the following:

SUPPLEMENTAL INFORMATION

Supplemental information can be found online at https://doi.org/10.1016/j.cell.2022.03.044.

ACKNOWLEDGMENTS

We acknowledge Chen Dong and Xiaohu Wang (Tsinghua University) for providing fluorescent dye-conjugated antibodies. We thank Junyu Xiao (Peking University) for providing purified SARS-CoV-2 spike proteins and Jinghua Yan (Institute of Microbiology, Chinese Academy of Sciences) for providing RBD peptide pools. We thank the Laboratory Animal Center of Peking University for the maintenance of mice. We thank the HPLC Core at the National Center for Protein Sciences at Peking University (Beijing), particularly H. Li and G. Li for their technical help. We thank the flow cytometry Core at the National Center for Protein Sciences at Peking University (Beijing), particularly H. Lv, Y. Guo, H. Yang, and F. Wang for their technical help. This project was supported by funds from National Key R&D Program of China (2020YFA0707800 to W.W., 2020YFA0707600 to Z.Z.), the Beijing Municipal Science & Technology Commission (Z181100001318009 to W.W.), the National Science Foundation of China (31930016 to W.W.), the Beijing Advanced Innovation Center for Genomics at Peking University (to W.W). and the Peking-Tsinghua Center for Life Sciences (to W.W.), the National Science Foundation of China (31870893 to Z.Z.), the National Major Science & Technology Project for Control and Prevention of Major Infectious Diseases in China (2018ZX10301401 to Z.Z.), and the Fellowship of China National Postdoctoral Program for Innovative Talents (BX20200010 to L.Q.).

AUTHOR CONTRIBUTIONS

W.W. conceived and supervised this project. W.W., L.Q., Z.Y., and Y.S. designed the experiments. L.Q., Z.Y., Y.S., L.L., F.C., Y.X., Z.W., and H.T. performed the preparation of circRNA vaccines, mouse vaccination experiments, detection experiments, and data collection with the help of X.Z., F.T., C.W., A.Y., Y.C., Z.Z., X.S.X., and W.W. L.Q., Z.Y., Y.S., X.X., and X.D. performed the SARS-CoV-2 Beta variant challenge experiments in mice and related detection experiments with the help of Z.Z., L.G., Jianwei Wang, and W.W.

L.Q., Z.Y., Y.S., and S. Lu performed the rhesus macaque experiments and related detection experiments with the help of C.Y., C.T., Y.Y., W.Y., Junbin Wang, Y.Z., Q.H., X.P., and W.W. The VSV-based SARS-CoV-2 pseudovirus was produced by S. Liu, W.H., and Y.W. L.Q., Z.Y., Y.S., Z.Z., and W.W. wrote the manuscript with the help from all other authors.

DECLARATION OF INTERESTS

Patents related to the data presented have been filed. W.W. is the founder of Therorna, Inc.

Received: January 12, 2022
Revised: March 11, 2022
Accepted: March 30, 2022
Published: April 1, 2022

REFERENCES

Alameh, M.G., Tombácz, I., Bettini, E., Lederer, K., Sittplangkoon, C., Wilmore, J.R., Gaudette, B.T., Soliman, O.Y., Pine, M., Hicks, P., et al. (2021). Lipid nanoparticles enhance the efficacy of mRNA and protein subunit vaccines by inducing robust T follicular helper cell and humoral responses. Immunity *54*, 2877–2892.e7.

Bangaru, S., Ozorowski, G., Turner, H.L., Antanasijevic, A., Huang, D., Wang, X., Torres, J.L., Diedrich, J.K., Tian, J.H., Portnoff, A.D., et al. (2020). Structural analysis of full-length SARS-CoV-2 spike protein from an advanced vaccine candidate. Science *370*, 1089–1094.

Barnes, C.O., Jette, C.A., Abernathy, M.E., Dam, K.A., Esswein, S.R., Gristick, H.B., Malyutin, A.G., Sharaf, N.G., Huey-Tubman, K.E., Lee, Y.E., et al. (2020). SARS-CoV-2 neutralizing antibody structures inform therapeutic strategies. Nature *588*, 682–687.

Boutros, C., Tarhini, A., Routier, E., Lambotte, O., Ladurie, F.L., Carbonnel, F., Izzeddine, H., Marabelle, A., Champiat, S., Berdelou, A., et al. (2016). Safety profiles of anti-CTLA-4 and anti-PD-1 antibodies alone and in combination. Nat. Rev. Clin. Oncol. *13*, 473–486.

Bouwman, K.M., Tomris, I., Turner, H.L., van der Woude, R., Shamorkina, T.M., Bosman, G.P., Rockx, B., Herfst, S., Snijder, J., Haagmans, B.L., et al. (2021). Multimerization- and glycosylation-dependent receptor binding of SARS-CoV-2 spike proteins. PLoS Pathog. *17*, e1009282.

Cameroni, E., Bowen, J.E., Rosen, L.E., Saliba, C., Zepeda, S.K., Culap, K., Pinto, D., VanBlargan, L.A., De Marco, A., di Iulio, J., et al. (2022). Broadly neutralizing antibodies overcome SARS-CoV-2 Omicron antigenic shift. Nature *602*, 664–670.

Cao, Y., Su, B., Guo, X., Sun, W., Deng, Y., Bao, L., Zhu, Q., Zhang, X., Zheng, Y., Geng, C., et al. (2020). Potent neutralizing antibodies against SARS-CoV-2 identified by high-throughput single-cell sequencing of convalescent patients' B cells. Cell *182*, 73–84.e16.

Cao, Y., Wang, J., Jian, F., Xiao, T., Song, W., Yisimayi, A., Huang, W., Li, Q., Wang, P., An, R., et al. (2021). Omicron escapes the majority of existing SARS-CoV-2 neutralizing antibodies. Nature *602*, 657–663.

Cele, S., Jackson, L., Khoury, D.S., Khan, K., Moyo-Gwete, T., Tegally, H., San, J.E., Cromer, D., Scheepers, C., Amoako, D., et al. (2022). Omicron extensively but incompletely escapes Pfizer BNT162b2 neutralization. Nature *602*, 654–656.

Chan, K.K., Dorosky, D., Sharma, P., Abbasi, S.A., Dye, J.M., Kranz, D.M., Herbert, A.S., and Procko, E. (2020). Engineering human ACE2 to optimize binding to the spike protein of SARS coronavirus 2. Science *369*, 1261–1265.

Chen, L.L. (2016). The biogenesis and emerging roles of circular RNAs. Nat. Rev. Mol. Cell Biol. *17*, 205–211.

Chen, Q., Huang, X.Y., Sun, M.X., Li, R.T., Gu, H., Tian, Y., Zhang, R.R., Luo, D., Zhou, C., Zhang, Y., et al. (2021). Transient acquisition of cross-species infectivity during the evolution of SARS-CoV-2. Natl. Sci. Rev. *8*, nwab167.

Chen, Y.G., Chen, R., Ahmad, S., Verma, R., Kasturi, S.P., Amaya, L., Broughton, J.P., Kim, J., Cadena, C., Pulendran, B., et al. (2019). N6-methyladenosine modification controls circular RNA immunity. Mol. Cell *76*, 96–109.e9.

Corbett, K.S., Edwards, D.K., Leist, S.R., Abiona, O.M., Boyoglu-Barnum, S., Gillespie, R.A., Himansu, S., Schäfer, A., Ziwawo, C.T., DiPiazza, A.T., et al. (2020a). SARS-CoV-2 mRNA vaccine design enabled by prototype pathogen preparedness. Nature *586*, 567–571.

Corbett, K.S., Flynn, B., Foulds, K.E., Francica, J.R., Boyoglu-Barnum, S., Werner, A.P., Flach, B., O'Connell, S., Bock, K.W., Minai, M., et al. (2020b). Evaluation of the mRNA-1273 vaccine against SARS-CoV-2 in nonhuman primates. N. Engl. J. Med. *383*, 1544–1555.

Dai, L., Zheng, T., Xu, K., Han, Y., Xu, L., Huang, E., An, Y., Cheng, Y., Li, S., Liu, M., et al. (2020). A universal design of *Betacoronavirus* vaccines against COVID-19, MERS, and SARS. Cell *182*, 722–733.e11.

Dejnirattisai, W., Huo, J., Zhou, D., Zahradník, J., Supasa, P., Liu, C., Duyvesteyn, H.M.E., Ginn, H.M., Mentzer, A.J., Tuekprakhon, A., et al. (2022). SARS-CoV-2 Omicron-B.1.1.529 leads to widespread escape from neutralizing antibody responses. Cell *185*, 467–484.e15.

Dejnirattisai, W., Jumnainsong, A., Onsirisakul, N., Fitton, P., Vasanawathana, S., Limpitikul, W., Puttikhunt, C., Edwards, C., Duangchinda, T., Supasa, S., et al. (2010). Cross-reacting antibodies enhance dengue virus infection in humans. Science *328*, 745–748.

Dowd, K.A., and Pierson, T.C. (2011). Antibody-mediated neutralization of flaviviruses: a reductionist view. Virology *411*, 306–315.

Du, S., Cao, Y., Zhu, Q., Yu, P., Qi, F., Wang, G., Du, X., Bao, L., Deng, W., Zhu, H., et al. (2020). Structurally resolved SARS-CoV-2 antibody shows high efficacy in severely infected hamsters and provides a potent cocktail pairing strategy. Cell *183*, 1013–1023.e13.

Durymanov, M., and Reineke, J. (2018). Non-viral delivery of nucleic acids: insight Into mechanisms of overcoming intracellular barriers. Front. Pharmacol. *9*, 971.

Enuka, Y., Lauriola, M., Feldman, M.E., Sas-Chen, A., Ulitsky, I., and Yarden, Y. (2016). Circular RNAs are long-lived and display only minimal early alterations in response to a growth factor. Nucleic Acids Res. *44*, 1370–1383.

Fenton, O.S., Kauffman, K.J., McClellan, R.L., Appel, E.A., Dorkin, J.R., Tibbitt, M.W., Heartlein, M.W., DeRosa, F., Langer, R., and Anderson, D.G. (2016). Bioinspired alkenyl amino alcohol ionizable lipid materials for highly potent in vivo mRNA delivery. Adv. Mater. *28*, 2939–2943.

Fischer, J.W., and Leung, A.K. (2017). CircRNAs: a regulator of cellular stress. Crit. Rev. Biochem. Mol. Biol. *52*, 220–233.

Gao, Q., Bao, L., Mao, H., Wang, L., Xu, K., Yang, M., Li, Y., Zhu, L., Wang, N., Lv, Z., et al. (2020). Development of an inactivated vaccine candidate for SARS-CoV-2. Science *369*, 77–81.

Gao, X., Xia, X., Li, F., Zhang, M., Zhou, H., Wu, X., Zhong, J., Zhao, Z., Zhao, K., Liu, D., et al. (2021). Circular RNA-encoded oncogenic E-cadherin variant promotes glioblastoma tumorigenicity through activation of EGFR-STAT3 signalling. Nat. Cell Biol. *23*, 278–291.

Garcia-Beltran, W.F., St Denis, K.J., Hoelzemer, A., Lam, E.C., Nitido, A.D., Sheehan, M.L., Berrios, C., Ofoman, O., Chang, C.C., Hauser, B.M., et al. (2022). mRNA-based COVID-19 vaccine boosters induce neutralizing immunity against SARS-CoV-2 Omicron variant. Cell *185*, 457–466.e4.

Glasgow, A., Glasgow, J., Limonta, D., Solomon, P., Lui, I., Zhang, Y., Nix, M.A., Rettko, N.J., Zha, S., Yamin, R., et al. (2020). Engineered ACE2 receptor traps potently neutralize SARS-CoV-2. Proc. Natl. Acad. Sci. USA *117*, 28046–28055.

Graham, B.S. (2020). Rapid COVID-19 vaccine development. Science *368*, 945–946.

Gu, H., Chen, Q., Yang, G., He, L., Fan, H., Deng, Y.Q., Wang, Y., Teng, Y., Zhao, Z., Cui, Y., et al. (2020). Adaptation of SARS-CoV-2 in BALB/c mice for testing vaccine efficacy. Science *369*, 1603–1607.

Halstead, S.B., and O'Rourke, E.J. (1977). Dengue viruses and mononuclear phagocytes. I. Infection enhancement by non-neutralizing antibody. J. Exp. Med. *146*, 201–217.

He, X., and Xu, C. (2020). Immune checkpoint signaling and cancer immunotherapy. Cell Res. *30*, 660–669.

Hoffmann, M., Kleine-Weber, H., Schroeder, S., Krüger, N., Herrler, T., Erichsen, S., Schiergens, T.S., Herrler, G., Wu, N.H., Nitsche, A., et al. (2020). SARS-CoV-2 cell entry depends on ACE2 and TMPRSS2 and is blocked by a clinically proven protease inhibitor. Cell *181*, 271–280.e8.

Hsieh, C.L., Goldsmith, J.A., Schaub, J.M., DiVenere, A.M., Kuo, H.C., Javanmardi, K., Le, K.C., Wrapp, D., Lee, A.G., Liu, Y., et al. (2020). Structure-based design of prefusion-stabilized SARS-CoV-2 spikes. Science *369*, 1501–1505.

Huang, Q., Ji, K., Tian, S., Wang, F., Huang, B., Tong, Z., Tan, S., Hao, J., Wang, Q., Tan, W., et al. (2021). A single-dose mRNA vaccine provides a long-term protection for hACE2 transgenic mice from SARS-CoV-2. Nat. Commun. *12*, 776.

Ickenstein, L.M., and Garidel, P. (2019). Lipid-based nanoparticle formulations for small molecules and RNA drugs. Expert Opin. Drug Deliv. *16*, 1205–1226.

Jackson, N.A.C., Kester, K.E., Casimiro, D., Gurunathan, S., and DeRosa, F. (2020). The promise of mRNA vaccines: a biotech and industrial perspective. npj Vaccines *5*, 11.

Karikó, K., Buckstein, M., Ni, H., and Weissman, D. (2005). Suppression of RNA recognition by toll-like receptors: the impact of nucleoside modification and the evolutionary origin of RNA. Immunity *23*, 165–175.

Karim, S.S.A., and Karim, Q.A. (2021). Omicron SARS-CoV-2 variant: a new chapter in the COVID-19 pandemic. Lancet *398*, 2126–2128.

Khan, K., Karim, F., Cele, S., San, J.E., Lustig, G., Tegally, H., Bernstein, M., Ganga, Y., Jule, Z., Reedoy, K., et al. (2021). Omicron infection enhances neutralizing immunity against the Delta variant. Preprint at medRxiv, 2021.12.27.21268439.

Kim, D., Lee, J.Y., Yang, J.S., Kim, J.W., Kim, V.N., and Chang, H. (2020). The architecture of SARS-CoV-2 transcriptome. Cell *181*, 914–921.e10.

Koenig, P.A., Das, H., Liu, H., Kümmerer, B.M., Gohr, F.N., Jenster, L.M., Schiffelers, L.D.J., Tesfamariam, Y.M., Uchima, M., Wuerth, J.D., et al. (2021). Structure-guided multivalent nanobodies block SARS-CoV-2 infection and suppress mutational escape. Science *371*, eabe6230.

Kou, Y., Xu, Y., Zhao, Z., Liu, J., Wu, Y., You, Q., Wang, L., Gao, F., Cai, L., and Jiang, C. (2017). Tissue plasminogen activator (tPA) signal sequence enhances immunogenicity of MVA-based vaccine against tuberculosis. Immunol. Lett. *190*, 51–57.

Krammer, F. (2020). SARS-CoV-2 vaccines in development. Nature *586*, 516–527.

Kristensen, L.S., Andersen, M.S., Stagsted, L.V.W., Ebbesen, K.K., Hansen, T.B., and Kjems, J. (2019). The biogenesis, biology and characterization of circular RNAs. Nat. Rev. Genet. *20*, 675–691.

Laczkó, D., Hogan, M.J., Toulmin, S.A., Hicks, P., Lederer, K., Gaudette, B.T., Castaño, D., Amanat, F., Muramatsu, H., Oguin, T.H., 3rd., et al. (2020). A single immunization with nucleoside-modified mRNA vaccines elicits strong cellular and humoral immune responses against SARS-CoV-2 in mice. Immunity *53*, 724–732.e7.

Legnini, I., Di Timoteo, G., Rossi, F., Morlando, M., Briganti, F., Sthandier, O., Fatica, A., Santini, T., Andronache, A., Wade, M., et al. (2017). Circ-ZNF609 is a circular RNA that can be translated and functions in myogenesis. Mol. Cell *66*, 22–37.e9.

Linsky, T.W., Vergara, R., Codina, N., Nelson, J.W., Walker, M.J., Su, W., Barnes, C.O., Hsiang, T.Y., Esser-Nobis, K., Yu, K., et al. (2020). De novo design of potent and resilient hACE2 decoys to neutralize SARS-CoV-2. Science *370*, 1208–1214.

Liu, C.X., Guo, S.K., Nan, F., Xu, Y.F., Yang, L., and Chen, L.L. (2022). RNA circles with minimized immunogenicity as potent PKR inhibitors. Mol. Cell *82*, 420–434.e6.

Liu, L., Iketani, S., Guo, Y., Chan, J.F.W., Wang, M., Liu, L., Luo, Y., Chu, H., Huang, Y., Nair, M.S., et al. (2022). Striking antibody evasion manifested by the Omicron variant of SARS-CoV-2. Nature *602*, 676–681.

Liu, B., Lin, Y., Yan, J., Yao, J., Liu, D., Ma, W., Wang, J., Liu, W., Wang, C., Zhang, L., and Qi, H. (2021). Affinity-coupled CCL22 promotes positive selection in germinal centres. Nature *592*, 133–137.

Lustig, Y., Zuckerman, N., Nemet, I., Atari, N., Kliker, L., Regev-Yochay, G., Sapir, E., Mor, O., Alroy-Preis, S., Mendelson, E., and Mandelboim, M. (2021). Neutralising capacity against Delta (B.1.617.2) and other variants of concern following Comirnaty (BNT162b2, BioNTech/Pfizer) vaccination in health care workers, Israel. Euro Surveill. *26*, 2100557.

Martínez-Vega, R.A., Carrasquila, G., Luna, E., and Ramos-Castañeda, J. (2017). ADE and dengue vaccination. Vaccine *35*, 3910–3912.

Memczak, S., Jens, M., Elefsinioti, A., Torti, F., Krueger, J., Rybak, A., Maier, L., Mackowiak, S.D., Gregersen, L.H., Munschauer, M., et al. (2013). Circular RNAs are a large class of animal RNAs with regulatory potency. Nature *495*, 333–338.

Montagutelli, X., Prot, M., Levillayer, L., Salazar, E.B., Jouvion, G., Conquet, L., Donati, F., Albert, M., Gambaro, F., Behillil, S., et al. (2021). Variants with the N501Y mutation extend SARS-CoV-2 host range to mice, with contact transmission. Preprint at bioRxiv. https://doi.org/10.1101/2021.03.18.436013.

Muik, A., Wallisch, A.K., Sänger, B., Swanson, K.A., Mühl, J., Chen, W., Cai, H., Maurus, D., Sarkar, R., Türeci, Ö., et al. (2021). Neutralization of SARS-CoV-2 lineage B.1.1.7 pseudovirus by BNT162b2 vaccine-elicited human sera. Science *371*, 1152–1153.

Mukhopadhyay, S., Vander Heiden, M.G., and McCormick, F. (2021). The metabolic landscape of RAS-driven Cancers from biology to therapy. Nat. Cancer *2*, 271–283.

Mullard, A. (2020). COVID-19 vaccine development pipeline gears up. Lancet *395*, 1751–1752.

Ou, X., Liu, Y., Lei, X., Li, P., Mi, D., Ren, L., Guo, L., Guo, R., Chen, T., Hu, J., et al. (2020). Characterization of spike glycoprotein of SARS-CoV-2 on virus entry and its immune cross-reactivity with SARS-CoV. Nat. Commun. *11*, 1620.

Papanikolopoulou, K., van Raaij, M.J., and Mitraki, A. (2008). Creation of hybrid nanorods from sequences of natural trimeric fibrous proteins using the fibritin trimerization motif. Methods Mol. Biol. *474*, 15–33.

Pardi, N., Hogan, M.J., Pelc, R.S., Muramatsu, H., Andersen, H., DeMaso, C.R., Dowd, K.A., Sutherland, L.L., Scearce, R.M., Parks, R., et al. (2017). Zika virus protection by a single low-dose nucleoside-modified mRNA vaccination. Nature *543*, 248–251.

Pardi, N., Hogan, M.J., Porter, F.W., and Weissman, D. (2018). mRNA vaccines - a new era in vaccinology. Nat. Rev. Drug Discov. *17*, 261–279.

Planas, D., Saunders, N., Maes, P., Guivel-Benhassine, F., Planchais, C., Buchrieser, J., Bolland, W.-H., Porrot, F., Staropoli, I., Lemoine, F., et al. (2022). Considerable escape of SARS-CoV-2 Omicron to antibody neutralization. Nature *602*, 671–675.

Planas, D., Veyer, D., Baidaliuk, A., Staropoli, I., Guivel-Benhassine, F., Rajah, M.M., Planchais, C., Porrot, F., Robillard, N., Puech, J., et al. (2021). Reduced sensitivity of SARS-CoV-2 variant Delta to antibody neutralization. Nature *596*, 276–280.

Rey, F.A., Stiasny, K., Vaney, M.C., Dellarole, M., and Heinz, F.X. (2018). The bright and the dark side of human antibody responses to flaviviruses: lessons for vaccine design. EMBO Rep. *19*, 206–224.

Richner, J.M., Himansu, S., Dowd, K.A., Butler, S.L., Salazar, V., Fox, J.M., Julander, J.G., Tang, W.W., Shresta, S., Pierson, T.C., et al. (2017). Modified mRNA vaccines protect against Zika virus infection. Cell *169*, 176.

Routhu, N.K., Cheedarla, N., Bollimpelli, V.S., Gangadhara, S., Edara, V.V., Lai, L., Sahoo, A., Shiferaw, A., Styles, T.M., Floyd, K., et al. (2021). SARS-CoV-2 RBD trimer protein adjuvanted with Alum-3M-052 protects from SARS-CoV-2 infection and immune pathology in the lung. Nat. Commun. *12*, 3587.

Sabapathy, K., and Lane, D.P. (2018). Therapeutic targeting of p53: all mutants are equal, but some mutants are more equal than others. Nat. Rev. Clin. Oncol. *15*, 13–30.

Sahin, U., Muik, A., Derhovanessian, E., Vogler, I., Kranz, L.M., Vormehr, M., Baum, A., Pascal, K., Quandt, J., Maurus, D., et al. (2020). COVID-19 vaccine

BNT162b1 elicits human antibody and TH1 T cell responses. Nature *586*, 594–599.

Sanchez-Felipe, L., Vercruysse, T., Sharma, S., Ma, J., Lemmens, V., Van Looveren, D., Arkalagud Javarappa, M.P., Boudewijns, R., Malengier-Devlies, B., Liesenborghs, L., et al. (2021). A single-dose live-attenuated YF17D-vectored SARS-CoV-2 vaccine candidate. Nature *590*, 320–325.

Schoof, M., Faust, B., Saunders, R.A., Sangwan, S., Rezelj, V., Hoppe, N., Boone, M., Billesbølle, C.B., Puchades, C., Azumaya, C.M., et al. (2020). An ultrapotent synthetic nanobody neutralizes SARS-CoV-2 by stabilizing inactive Spike. Science *370*, 1473–1479.

Sette, A., and Crotty, S. (2021). Adaptive immunity to SARS-CoV-2 and COVID-19. Cell *184*, 861–880.

Shang, J., Wan, Y., Luo, C., Ye, G., Geng, Q., Auerbach, A., and Li, F. (2020). Cell entry mechanisms of SARS-CoV-2. Proc. Natl. Acad. Sci. USA *117*, 11727–11734.

Tai, W., Zhang, X., Drelich, A., Shi, J., Hsu, J.C., Luchsinger, L., Hillyer, C.D., Tseng, C.K., Jiang, S., and Du, L. (2020). A novel receptor-binding domain (RBD)-based mRNA vaccine against SARS-CoV-2. Cell Res. *30*, 932–935.

Takano, T., Yamada, S., Doki, T., and Hohdatsu, T. (2019). Pathogenesis of oral type I feline infectious peritonitis virus (FIPV) infection: antibody-dependent enhancement infection of cats with type I FIPV via the oral route. J. Vet. Med. Sci. *81*, 911–915.

Torgovnick, J. (2021). Effectiveness of COVID-19 vaccines against the B.1.617.2 (Delta) variant. N. Engl. J. Med. *385*, e92.

Uddin, M.N., and Roni, M.A. (2021). Challenges of storage and stability of mRNA-based COVID-19 vaccines. Vaccines (Basel) *9*, 1033.

van Doremalen, N., Lambe, T., Spencer, A., Belij-Rammerstorfer, S., Purushotham, J.N., Port, J.R., Avanzato, V.A., Bushmaker, T., Flaxman, A., Ulaszewska, M., et al. (2020). ChAdOx1 nCoV-19 vaccine prevents SARS-CoV-2 pneumonia in rhesus macaques. Nature *586*, 578–582.

V'Kovski, P., Kratzel, A., Steiner, S., Stalder, H., and Thiel, V. (2021). Coronavirus biology and replication: implications for SARS-CoV-2. Nat. Rev. Microbiol. *19*, 155–170.

Vogel, A.B., Kanevsky, I., Che, Y., Swanson, K.A., Muik, A., Vormehr, M., Kranz, L.M., Walzer, K.C., Hein, S., Guler, A., et al. (2021). BNT162b vaccines protect rhesus macaques from SARS-CoV-2. Nature *592*, 283–289.

Walls, A.C., Park, Y.J., Tortorici, M.A., Wall, A., McGuire, A.T., and Veesler, D. (2020). Structure, function, and antigenicity of the SARS-CoV-2 spike glycoprotein. Cell *181*, 281–292.e6.

Wang, P., Nair, M.S., Liu, L., Iketani, S., Luo, Y., Guo, Y., Wang, M., Yu, J., Zhang, B., Kwong, P.D., et al. (2021a). Antibody resistance of SARS-CoV-2 variants B.1.351 and B.1.1.7. Nature *593*, 130–135.

Wang, Z., Schmidt, F., Weisblum, Y., Muecksch, F., Barnes, C.O., Finkin, S., Schaefer-Babajew, D., Cipolla, M., Gaebler, C., Lieberman, J.A., et al. (2021b). mRNA vaccine-elicited antibodies to SARS-CoV-2 and circulating variants. Nature *592*, 616–622.

Wen, J., Cheng, Y., Ling, R., Dai, Y., Huang, B., Huang, W., Zhang, S., and Jiang, Y. (2020). Antibody-dependent enhancement of coronavirus. Int. J. Infect. Dis. *100*, 483–489.

Wesselhoeft, R.A., Kowalski, P.S., and Anderson, D.G. (2018). Engineering circular RNA for potent and stable translation in eukaryotic cells. Nat. Commun. *9*, 2629.

Wesselhoeft, R.A., Kowalski, P.S., Parker-Hale, F.C., Huang, Y., Bisaria, N., and Anderson, D.G. (2019). RNA circularization diminishes immunogenicity and can extend translation duration *in vivo*. Mol. Cell *74*, 508–520.e4.

Wrapp, D., Wang, N., Corbett, K.S., Goldsmith, J.A., Hsieh, C.L., Abiona, O., Graham, B.S., and McLellan, J.S. (2020). Cryo-EM structure of the 2019-nCoV spike in the prefusion conformation. Science *367*, 1260–1263.

Wu, F., Zhao, S., Yu, B., Chen, Y.M., Wang, W., Song, Z.G., Hu, Y., Tao, Z.W., Tian, J.H., Pei, Y.Y., et al. (2020). A new coronavirus associated with human respiratory disease in China. Nature *579*, 265–269.

Xiang, Y., Nambulli, S., Xiao, Z., Liu, H., Sang, Z., Duprex, W.P., Schneidman-Duhovny, D., Zhang, C., and Shi, Y. (2020). Versatile and multivalent nanobodies efficiently neutralize SARS-CoV-2. Science *370*, 1479–1484.

Yan, R., Zhang, Y., Li, Y., Xia, L., Guo, Y., and Zhou, Q. (2020). Structural basis for the recognition of SARS-CoV-2 by full-length human ACE2. Science *367*, 1444–1448.

Yang, J., Wang, W., Chen, Z., Lu, S., Yang, F., Bi, Z., Bao, L., Mo, F., Li, X., Huang, Y., et al. (2020). A vaccine targeting the RBD of the S protein of SARS-CoV-2 induces protective immunity. Nature *586*, 572–577.

Yang, Y., Fan, X., Mao, M., Song, X., Wu, P., Zhang, Y., Jin, Y., Yang, Y., Chen, L.L., Wang, Y., et al. (2017). Extensive translation of circular RNAs driven by N(6)-methyladenosine. Cell Res. *27*, 626–641.

Yu, J., Tostanoski, L.H., Peter, L., Mercado, N.B., McMahan, K., Mahrokhian, S.H., Nkolola, J.P., Liu, J., Li, Z., Chandrashekar, A., et al. (2020). DNA vaccine protection against SARS-CoV-2 in rhesus macaques. Science *369*, 806–811.

Zhang, M., Huang, N., Yang, X., Luo, J., Yan, S., Xiao, F., Chen, W., Gao, X., Zhao, K., Zhou, H., et al. (2018a). A novel protein encoded by the circular form of the SHPRH gene suppresses glioma tumorigenesis. Oncogene *37*, 1805–1814.

Zhang, M., Zhao, K., Xu, X., Yang, Y., Yan, S., Wei, P., Liu, H., Xu, J., Xiao, F., Zhou, H., et al. (2018b). A peptide encoded by circular form of LINC-PINT suppresses oncogenic transcriptional elongation in glioblastoma. Nat. Commun. *9*, 4475.

Zhang, N.N., Li, X.F., Deng, Y.Q., Zhao, H., Huang, Y.J., Yang, G., Huang, W.J., Gao, P., Zhou, C., Zhang, R.R., et al. (2020). A thermostable mRNA vaccine against COVID-19. Cell *182*, 1271–1283.e16.

Zhang, X.O., Wang, H.B., Zhang, Y., Lu, X., Chen, L.L., and Yang, L. (2014). Complementary sequence-mediated exon circularization. Cell *159*, 134–147.

Zhou, P., Yang, X.L., Wang, X.G., Hu, B., Zhang, L., Zhang, W., Si, H.R., Zhu, Y., Li, B., Huang, C.L., et al. (2020). A pneumonia outbreak associated with a new coronavirus of probable bat origin. Nature *579*, 270–273.

Zhu, F.C., Li, Y.H., Guan, X.H., Hou, L.H., Wang, W.J., Li, J.X., Wu, S.P., Wang, B.S., Wang, Z., Wang, L., et al. (2020). Safety, tolerability, and immunogenicity of a recombinant adenovirus type-5 vectored COVID-19 vaccine: a dose-escalation, open-label, non-randomised, first-in-human trial. Lancet *395*, 1845–1854.

STAR★METHODS

KEY RESOURCES TABLE

REAGENT or RESOURCE	SOURCE	IDENTIFIER
Antibodies		
SARS-CoV-2 Spike RBD Rabbit pAb	ABclonal	Cat#A20135; RRID:AB_2862927
Mouse monoclonal GFP antibody	Beyotime	Cat#AG281; RRID:AB_2895206
Anti-β-Tubulin Mouse Monoclonal Antibody	Cwbio	Cat#CW0098M; RRID:AB_2814800
Anti-Mouse IgG-Peroxidase antibody in rabbit	Merck	Cat#A9044; RRID:AB_258431
HRP-Monoclonal Mouse Anti-Monkey IgG	Immunoway	Cat#RS030204
Goat Anti-Mouse IgG1 (HRP)	Abcam	Cat#ab97240; RRID:AB_10695944
Goat Anti-Mouse IgG2a (HRP)	Abcam	Cat#ab97245; RRID:AB_10680049
Goat Anti-Mouse IgG2c (HRP)	Abcam	Cat#ab97255; RRID:AB_10680258
Anti-Mouse CD3 Monoclonal Antibody, BV650	BioLegend	Cat#100229; RRID:AB_11204249
Anti-Mouse CD4 Monoclonal Antibody, BV785	BioLegend	Cat#100552; RRID:AB_2563053
Anti-Mouse CD8 Monoclonal Antibody, APC/ Cyanine7	BioLegend	Cat#100714; RRID:AB_312753
Anti-Mouse CD44 Monoclonal Antibody, FITC	BioLegend	Cat#103006; RRID:AB_312957
Anti-Mouse CD62L Monoclonal Antibody, BV711	BioLegend	Cat#104445; RRID:AB_2564215
Anti-Mouse IFN-γ Monoclonal Antibody, APC	BioLegend	Cat#505810; RRID:AB_315404
Anti-Mouse IL-2 Monoclonal Antibody, AF700	BioLegend	Cat#503818; RRID:AB_528931
Anti-Mouse TNF-α Monoclonal Antibody, PE/Cyanine7	BioLegend	Cat#506324; RRID:AB_2256076
Anti-Mouse IL-4 Monoclonal Antibody, PE	BioLegend	Cat#504104; RRID:AB_315318
Virus strains		
Lenti-based SARS-CoV-2 pseudovirus	This paper	N/A
Authentic SARS-CoV-2 virus	This paper	N/A
VSV-based SARS-CoV-2 pseudovirus	Institute for Biological Product Control, National Institutes for Food and Drug Control (NIFDC)	N/A
Chemicals, peptides, and recombinant proteins		
Lipofectamine MessengerMax	Thermo Fisher Scientific	Cat#LMRNA003
SARS-CoV-2 B.1.1.529 (Omicron) S1+S2 trimer Protein (ECD, His Tag)	Sino Biological	Cat#40589-V08H26
SARS-CoV-2 (2019-nCoV) Spike RBD-His Recombinant Protein	Sino Biological	Cat#40592-V08H
SARS-CoV-2 (2019-nCoV) Spike RBD (K417N, E484K, N501Y)-His Recombinant Protein	Sino Biological	Cat#40592-V08H85
SARS-CoV-2 Spike RBD (L452R, T478K) Protein (His Tag)	Sino Biological	Cat#40592-V08H90
SARS-CoV-2 B.1.1.529 (Omicron) Spike RBD Protein (His Tag)	Sino Biological	Cat#40592-V08H121

(*Continued on next page*)

Continued

REAGENT or RESOURCE	SOURCE	IDENTIFIER
X tremeGENE HP DNA Transfection Reagent	Roche	Cat#6366236001
BRITELITE PLUS	Perkinelmer	Cat#6066769
Dulbecco's Modified Eagle Medium	Coring	Cat#10-013-CV
Fetal Bovine Serum	Biological Industries	Cat#C04001-500
Bovine Serum Albumin	Merck	Cat#B2064
ELISA Stop Solution	Bioss	Cat#C04-01003
1-Step Ultra TMB ELISA substrates	Thermo Fisher Scientific	Cat#34029
ELISA Washing Buffer (10x)	Bioss	Cat#C04-01004
RPMI 1640	Thermo Fisher Scientific	Cat#C11875500BT
eBioscience Cell Stimulation Cocktail (500x)	Thermo Fisher Scientific	Cat#00-4970-93
AIM-V Medium	Thermo Fisher Scientific	Cat#12055091
Phytohemagglutinin	Merck	Cat#L1668
PmeI	New England Biolabs	Cat#R0560L
DNase I	New England Biolabs	Cat#M0303L
RNase R	Epicentre	Cat#RNR07250
RNase H	New England Biolabs	Cat#M0297
T4 RNA Ligase 2	New England Biolabs	Cat#M0239
Quick CIP	New England Biolabs	Cat#M0525L
TB Green Premix Ex Taq II	TaKaRa	Cat#RR820A
HindIII-HF	New England Biolabs	Cat#R3104L
RNase Inhibitor, Murine	APExBIO	Cat#K1046
m7G(5')ppp(5')G RNA Cap Structure Analog	New England Biolabs	Cat#S1404S
Critical commercial assays		
SARS-CoV-2 Spike RBD Protein ELISA kit	ABclonal	Cat#RK04135
SARS-CoV-2 Surrogate Virus Neutralization Test Kit	GenScript	Cat#L00847A
Nano-Glo Luciferase Assay System	Promega	Cat#N1110
Monkey IFN-γ ELISpot PLUS kit (HRP)	Mabtech	Cat#3421M-4HPW-2
Monkey IL-2 ELISpot PLUS kit (HRP)	Mabtech	Cat#3445M-4HPW-2
Monkey IL-4 T cell ELISPOT kit	U-CyTech	Cat#CT128-PR5
Monkey IL-6 ELISA kit	Abcam	Cat#ab242233
Monkey MCP-1 ELISA kit	Cloud-clone	Cat#SEA087Si96T
Monkey TNF-α ELISA kit	Abcam	Cat#ab252354
Monkey IL-1β ELISA kit	Cloud-clone	Cat#SEA563Si96T
Monkey IFN-α ELISA kit	Chenglin	Cat#AD0081Mk
DNA Clean & Concentrator	Zymo Research	Cat#D4034
T7 High Yield RNA Synthesis Kit	New England Biolabs	Cat#E2040S
RNA Clean & Concentrator	Zymo Research	Cat#R1017
Monarch® RNA Cleanup Kit	New England Biolabs	Cat#T2040L
Zombie Aqua Fixable Viability Kit	BioLegend	Cat#423102
Fixation/Permeabilization Solution Kit with BD GolgiStop	Becton, Dickinson and Company	Cat#554715
Quant-it RiboGreen RNA Assay Kit	Thermo Fisher Scientific	Cat#R11490
Experimental models: Cell lines		
Human: HEK293T	This paper	N/A
Mouse: NIH3T3	This paper	N/A

(*Continued on next page*)

Continued

REAGENT or RESOURCE	SOURCE	IDENTIFIER
Human: Huh-7	This paper	N/A
Human: HEK293T-hACE2	Biodragon	Cat#BDAA0039
Human: A549-hACE2	This paper	N/A
Experimental models: Organisms/strains		
Mouse: BALB/c	Beijing Vital River Laboratory Animal Technology Co., Ltd	N/A
Rhesus macaque	National Kunming High-level Biosafety Primate Research Center, Institute of Medical Biology, Chinese Academy of Medical Sciences and Peking Union Medical College, Yunnan China.	N/A
Recombinant DNA		
pcircRNA backbone	This paper	N/A
psPAX2	Ou et al., 2020	N/A
pSpike	Ou et al., 2020	N/A
pLenti-Luc-GFP	Ou et al., 2020	N/A
Software and algorithms		
GraphPad Prism Version 8.0	Graphpad	https://www.graphpad.com/
Image Lab	Bio-Rad	N/A
FlowJo	BD	N/A

RESOURCE AVAILABILITY

Lead contact

Further information and requests for resources and reagents should be directed to and will be fulfilled by the lead contact, wswei@pku.edu.cn (W.W.).

Material availability

All unique reagents generated in this study, such as circRNA, mRNA and cell lines are available from the lead contact with a completed Material Transfer Agreement.

Data and code availability

All data and materials presented in this manuscript are available from the corresponding author (W.W.) upon a reasonable request under a completed Material Transfer Agreement. This paper does not report original code. Any additional information required to re-analyze the data reported in this work paper is available from the lead contact upon request. Additional Supplemental Items are available from Mendeley Data at https://doi.org/10.17632/vp2fskswfv.1.

EXPERIMENTAL MODEL AND SUBJECT DETAILS

Animals and ethics statement

The female BALB/c mice (6- to 8-week old) were ordered from Beijing Vital River Laboratory Animal Technology Co., Ltd. All mice were bred and kept under specific pathogen-free (SPF) conditions in the Laboratory Animal Center of Peking University. The animal experiments were approved by Peking University Laboratory Animal Center (Beijing) and undertaken in accordance with the National Institute of Health Guide for Care and Use of Laboratory Animals. All animal experiments with SARS-CoV-2 challenge were conducted under animal biosafety level 3 (ABSL3) facilities at the Institute of Pathogen Biology, Chinese Academy of Medical Sciences. All the animal experiments with SARS-CoV-2 challenge were reviewed and approved by the Committee on the Ethics of Animal Experiments of the Institute of Pathogen Biology, Chinese Academy of Medical Sciences.

The 2- to 4-year-old male rhesus macaque experiments were performed in the animal biosafety level 4 (ABSL-4) facility of the National Kunming High-level Biosafety Primate Research Center, Yunnan, China. All animal procedures were approved by the Institutional Animal Care and Use Committee of the Institute of Medical Biology, Chinese Academy of Medical Science. Commercial monkey chow treats and fruit were provided daily by trained personnel.

Cells and viruses

HEK293T, NIH3T3 and Huh-7 cell lines were maintained in our laboratory. The HEK293T-hACE2 cell line was ordered from Biodragon Inc. (#BDAA0039, Beijing, China). The A549-hACE2 cell line was generated in our laboratory. These mammalian cell lines were cultured in Dulbecco's Modified Eagle Medium (Corning, 10-013-CV) with 10% fetal bovine serum (FBS) (BI), supplemented with 1% penicillin–streptomycin in 5% CO_2 incubator at 37 °C. The Huh-7 cells were cultured with the methods previously described methods (Cao et al., 2020).

The production of lentivirus-based SARS-CoV-2 pseudovirus and neutralization assays were performed as described previously (Ou et al., 2020). Briefly, the SARS-CoV-2 pseudovirus was produced by cotransfecting plasmids psPAX2 (6 μg), pSpike (6 μg), and pLenti-Luc-GFP (6 μg) into HEK293T cells using X tremeGENE HP DNA Transfection Reagent (Roche) according to the manufacturer's instructions. Forty-eight hours after transfection, the supernatants containing pseudovirus particles were harvested and filtered through a 0.22-μm sterilized membrane for the neutralization assay as described below. The VSV-based pseudovirus of SARS-CoV-2 and its variants were described previously (Cao et al., 2020, 2021; Du et al., 2020). Authentic viruses were amplified from Vero-E6 cells and concentrated by an ultrafilter system via a 300 kD module (Millipore). Amplified SARS-CoV-2 was confirmed via RT–PCR, sequencing and transmission electronic microscopy, and titrated via plaque assay (10^6 PFU/ml).

METHOD DETAILS

Plasmid construction

The 5' homology arm sequence, 3' group I intron sequence, linker-1 sequence, IRES sequence, linker-2 sequence, 5' group I intron sequence and 3' homology arm sequence were PCR amplified and cloned into a plasmid backbone via the Gibson assembly strategy, generating the empty pcircRNA-EV backbone. Then, the SARS-CoV-2 RBD antigen, EGFP, nanobody or hACE2-decoy-coding sequence was PCR amplified and cloned into the pcircRNA-EV backbone, and the corresponding pcircRNA plasmids were constructed for the following IVT reaction.

Production and purification of circRNA

The production of circRNAs was performed according to previous reports (Wesselhoeft et al., 2018). Briefly, the circRNA precursors were synthesized via IVT from the linearized circRNA plasmid templates with the HiScribe™ T7 High Yield RNA Synthesis Kit (New England Biolabs, #E2040S). After IVT, the RNA products were treated with DNase I (New England Biolabs, #M0303S) for 30 min to digest the DNA templates. Optionally, after DNase I digestion, GTP was added to the reaction at a final concentration of 2 mM, and then the reactions were incubated at 55 °C for 15 min to catalyze the cyclization of circRNAs. Then, the RNA was column purified with the Monarch RNA Cleanup Kit (New England Biolabs, #T2040L). Then, the column-purified RNA was heated at 65 °C for 3 min and cooled on ice. The reactions were treated with RNase R (Epicenter, #RNR07250) at 37 °C for 15-30 min to further enrich the circRNAs. The RNase R-treated RNA was column purified. For optimized IVT reaction, circRNAs were directly column purified after IVT for further HPLC purification. The sequences of circRNAs produced via group I intron were provided in Table S1.

We used split IRES strategy to produce circular RNAs by T4 RNA ligase 2 (NEB, #M0239). To test the potential split sites in CVB3 IRES sequence, we analyzed the second structure of IRES. After multiple tests and screens, we were able to determine the split site of CVB3 IRES at the 385th nucleotide to allow T4 RNA ligase method for effective circularization. Then the circular RNA precursors were produced via *in vitro* transcription (NEB, E2040S) with added Guanosine monophosphates, and the RNA precursors were ligated by T4 RNA ligase 2 for 8 h at 25 °C. Finally, the ligated circular products were treated with RNase R to remove the linear RNA precursors. The sequences of circRNAs produced via T4 RNA ligases were provided in Table S2.

To further enrich the circRNAs, the purified RNase R-treated RNA was resolved with high-performance liquid chromatography (Agilent HPLC1260) using a 4.6 × 300 mm size-exclusion column with a particle size of 5 μm and pore size of 2000 Å (Sepax Technologies, #215980P-4630) in RNase-free TE buffer (Thermo, #T11493). The circRNA-enriched fractions were collected and then column purified. To further diminish the immunogenicity of the purified circRNAs, circRNAs were heated at 65 °C for 3 min, cooled on ice and subsequently treated with Quick CIP phosphatase (New England Biolabs, #M0525S). Finally, the circRNAs were column purified and concentrated with the RNA Clean & Concentrator Kit (ZYMO, #R1018).

Production and purification of mRNA

The production of mRNAs referred to the manufacturer's instructions. Briefly, we produced the mRNAs using the commercial HiScribe™ T7 High Yield RNA Synthesis Kit (NEB, #E2040S) according to the manufacturer's instructions with the linearized plasmids containing the 5'-UTR, RBD-coding region, 3'-UTR and -81-nt polyA elements. For 1mΨ-modified mRNA production, the 1-Methylpseudouridine-5-Triphosphate (TriLink, #N-1081-10) was used instead of the unmodified 5-Triphosphate for the production of 1mΨ-modified mRNA. The m7G(5')ppp(5')G RNA Cap Structure Analog (NEB, #S1404) was used for cotranscriptional capping of mRNAs according to the manufacturer's instructions. Final IVT products were column purified and concentrated with the RNA Clean & Concentrator Kit (ZYMO, #R1018). The sequence of mRNA was provided in Table S3.

RNase H cleavage assay

The purified circRNA^{RBD}, nicked linear RNA^{RBD} and linear precursor were incubated with RNase H (NEB, M0297L). Site-specific cleavage was performed in reactions containing 500 ng of the targeted RNAs, 50 pmol of the sense or antisense ssDNA probe and RNase H buffer in a total volume of 18 μl. After incubation at 50 °C for 10 min, 2 μl of RNase H was added to the reaction for 1 h at 37 °C. The sequence of the sense primer is 5'-TATTCTGTCCTCTAC-3', and the sequence of the antisense primer is 5'-GTA GAGGACAGAATA-3'.

RNase R cleavage assay

The nicked RNA^{RBD} or circRNA^{RBD} was heated at 65 °C for 3 min before cooled on ice. The RNase R (Epicentre, #RNR07250) was then added and incubated at 37 °C for 5 or 15 min. The reactions were stopped by adding 2 × RNA loading dye (NEB, #B0363S), and RNAs were resolved in agarose-gel electrophoresis.

CircRNA transfection *in vitro*

For circRNA transfection into HEK293T or NIH3T3 cells, 3×10^5 cells per well were seeded in 12-well plates. Two micrograms of circRNA was transfected into HEK293T or NIH3T3 cells using Lipofectamine MessengerMax (Invitrogen, #LMRNA003) according to the manufacturer's instructions. At 24-48 hr after transfection, the cell lysis and supernatant were collected for subsequent detection.

LNP encapsulation of circRNA

The circRNAs were encapsulated with lipid nanoparticles (LNPs) according to a previously described process (Ickenstein and Garidel, 2019). First, the circRNA was diluted with PNI Formulation Buffer (Precision NanoSystems, #NWW0043) to a final concentration of 170 μg/ml. Then, the lab-prepared or commercial LNP (Precision NanoSystems) were mixed with the circRNA solution at the volume ratio of 1:3 through the Ignite NxGen Cartridge (Precision NanoSystems, #NIT0002) using NanoAssemblr Ignite (Precision NanoSystems). Then the LNP-circRNA formulations were diluted 40-fold with 1×PBS buffer (pH 7.2∼7.4) and concentrated by ultrafiltration with Amicon® Ultra Centrifugal Filter Unit (Millipore). The concentration and encapsulation rate of circRNAs were measured by the Quant-it RiboGreen RNA Assay Kit (Invitrogen, #R11490). The size of LNP-circRNA particles was measured using dynamic light scattering on a Malvern Zetasizer Nano-ZS 300 (Malvern). Samples were irradiated with a red laser, and scattered light was detected. The results were analyzed to obtain an autocorrelation function using the software Zetasizer V7.13.

Quantitative determination of SARS-CoV-2 spike RBD expression *in vitro*

RBD expression in cell culture supernatants was quantified with a commercial SARS-CoV-2 spike RBD Protein ELISA kit (ABclonal, #RK04135) according to the manufacturer's instructions. The supernatants were diluted at proper ratio. Final concentrations of RBD were calculated based on the linear standard curve of absorbance at 450 nm, using 630 nm as a reference. Briefly, the detection wells were precoated with a monoclonal antibody specific for the spike RBD protein. After incubation with samples or standards at 37 °C for two hours, samples unbound to immobilized antibody were removed by washing steps. Then, RBD-specific antibodies were added to the wells for a one-hour incubation at 37 °C. After washing, the HRP substrates and stop solution were added, and the absorbance at 450 nm was measured using 630 nm as a reference.

Mouse vaccination and serum collection

For mouse vaccination, groups of 6- to 8-week-old female BALB/c mice were intramuscularly immunized with LNP-circRNA^{RBD} or a placebo (LNP only) in 100 μl using a 1-ml sterile syringe, and 2 or 3 weeks later, a second dose was administered to boost the immune responses. The sera of immunized mice were collected to detect the SARS-CoV-2-specific IgG endpoint GMTs and neutralizing antibodies as described below.

Antibody endpoint GMT measurement with ELISA

All immunized mouse serum samples were heat-inactivated at 56 °C for 30 min before use. The SARS-CoV-2-specific IgG antibody endpoint GMT was measured by ELISA. Briefly, serial 3-fold dilutions (in 1% BSA) of heat-inactivated sera, starting at 1:100, were added to 96-well plates (100 μl/well; Costar) coated with recombinant SARS-CoV-2 spike or RBD antigens (Sino Biological) and blocked with 1% BSA for 60 min at 37 °C. Then, after three washes with wash buffer, horseradish peroxidase HRP-conjugated rabbit anti-mouse IgG (Sigma) diluted in 1% BSA at a 1:10,000 ratio was added to the plates and incubated at 37 °C for 30 min. Then, the plates were washed 3 times with wash buffer and added to TMB substrates (100 μl/well) followed by incubation for 15-20 min. Then, the ELISA stop buffer was added to the plates. Finally, the absorbance (450/630 nm) was measured with an Infinite M200 (TECAN). The IgG endpoint GMTs were defined as the dilution fold, which emitted an optical density exceeding 3x background (without serum but the secondary antibody was added).

SARS-CoV-2 surrogate virus neutralization assay

The neutralizing activity of mouse serum samples was detected by a SARS-CoV-2 Surrogate Virus Neutralization Test Kit (L00847A, GenScript). Detections were performed according to the manufacturer's instructions. Serial 10-fold dilutions of heat-inactivated sera,

starting at 1:10, were incubated with HRP-conjugated RBD solutions at 37 °C for half an hour, and then the mixtures were placed in 96-well plates precoated with human ACE2 (hACE2) proteins and incubated for 15 min at 37 °C. After washing the TMB substrates, stop solution were added, and the absorbance (450/630 nm) was measured with an Infinite M200 (TECAN). The inhibition rates of serum samples were calculated according to the following formula. The 50% neutralization geometric mean titer (NT50) was determined using four-parameter nonlinear regression in Prism 8 (GraphPad).

$$\text{Inhibition rate} = (1 - \text{OD value of sample} / \text{OD value of negative control}) \times 100\%$$

Pseudovirus-based neutralization assay

For the determination of the NT50 of immunized mouse serum, HEK293T-hACE2 cells were seeded in 96-well plates (50,000 cells/well) and incubated for approximately 24 hr until reaching over 90% confluence in preparation for pseudovirus infection. The mouse serum was diluted 3-fold, starting at 1:40, and incubated with the SARS-CoV-2 pseudovirus (MOI ≈ 0.05) at 37 °C for 60 min. DMEM without serum was used as the negative control group. Then, the supernatant of HEK293T-hACE2 cells was removed, and a mixture of serum and pseudovirus was added to each well. Thirty-six to 48 hr later, the luciferase activity, which reflects the degree of SARS-CoV-2 pseudovirus transfection, was measured using the Nano-Glo Luciferase Assay System (Promega). The NT50 was defined as the fold dilution that achieved more than 50% inhibition of pseudovirus infection compared with the control group.

The sera were serially diluted using complete DMEM as the culture medium in 96-well white plates for a total of six gradients, and then the virus solution with ~1.3×10^4 TCID50 was added. Complete DMEM was used as the control group. After one hour of incubation in a 5% CO_2 incubator at 37 °C, Huh7 cells (100 μl/well) were added to the 96-well white plates, which were adjusted to a concentration of 2×10^5 cells/ml. After 24 h of incubation in a 5% CO_2 incubator at 37 °C, the culture supernatant was aspirated gently to leave 100 μl in each well, and then 100 μl of luciferase substrate (PerkinElmer, #6066769) was added to each well for the detection of luminescence using an Infinite M200 (TECAN). Relative luciferase units (RLU) were normalized to the corresponding DMEM control group, and the NT50 was determined by four-parameter nonlinear regression in Prism (GraphPad).

For the neutralization assay of circRNA^{nAB} or circRNA$^{ACE2\ decoys}$, HEK293T-hACE2 cells were seeded in 96-well plates (50,000 cells/well) and incubated for approximately 24 hr until they reached over 90% confluence. The pseudoviruses were preincubated with the supernatant of the circRNA^{nAB-} or circRNA^{ACE2} decoy$^-$transfected cells at 37 °C for 60 min and then added to cells in 96-well plates. Media were changed 24 hr after transduction. All cells were collected 48 hr after transduction. Luciferase activity was measured using the Nano-Glo Luciferase Assay System (Promega). The relative luminescence units were normalized to cells infected with the supernatant of cells transfected with circRNA^{EGFP}.

Authentic SARS-CoV-2 NT50 assay

A549-hACE2 cells were seeded in 96-well plates (20,000 cells/well) and incubated for approximately 24 hr until 90-100% confluence. The mouse serum was serially diluted 5-fold in DMEM, starting at 1:10. The diluted sera were then mixed with titrated virus in a 1:1 (vol/vol) ratio to generate a mixture containing ~2,000 PFU/well of viruses (MOI = 0.1), followed by an incubation at 37 °C for 1 hr. Then, the virus/serum mixtures were added to 24-well plates of A549-ACE2 cells supplemented with 100 μl of DMEM containing 10% FBS in each well. The supernatant and cell pellet precipitate were then collected, and the viral load was detected by RT–qPCR. Briefly, RNA was extracted from the cell pellet and reverse transcribed. SARS-CoV-2 RNA quantification was performed by RT–qPCR targeting the N gene of SARS-CoV-2 using a Roche LightCycler 96. The abundance of *GAPDH* was used as an internal reference. The NT50 was defined as the fold dilution that achieved inhibition of infection exceeding 50% of that of the control group.

Mouse challenge experiments

The mouse model for the SARS-CoV-2 Beta variant challenge has previously been characterized (Montagutelli et al., 2021). BALB/c mice immunized with circRNA$^{RBD\text{-}Beta}$ (50 μg) were challenged with 5×10^4 PFU SARS-CoV-2 Beta variant at 7 weeks after the boost. The body weights of the mice were recorded daily. At 3 days after the challenge, the immunized mice were sacrificed, and their lung tissues were collected to measure the viral RNA load, as described below.

Quantification of viral load in mice

The viral RNA load in the lung tissues of challenged mice was detected by quantitative RT–qPCR. Briefly, the lung tissues were collected and homogenized with stainless steel beads in TRIZOL (1 ml for each sample). The RNAs in tissues were then extracted and reverse transcribed. SARS-CoV-2 RNA quantification was performed by RT–qPCR targeting the N gene of SARS-CoV-2 using a Roche LightCycler 96. The abundance of *GAPDH* was used as an internal reference. The placebo group viral load was normalized to 100%.

T cell flow cytometry analysis

The splenocytes from each immunized mouse were cultured in R10 medium (RPMI 1640 supplemented with 1% Pen-Strep antibiotic, 10% HI-FBS) and stimulated with RBD peptide pools (Table S4) at a final concentration of 2 μg/ml for each peptide. Three hours later, the Golgi Stop transport inhibitor cocktail (BD) was added according to the manufacturer's instructions. Then, 6 hr later, cells from each group were pooled for stimulation with a cell stimulation cocktail (PMA/ionomycin) as a positive control. Following stimulation,

the cells were washed with PBS prior to staining with LIVE/DEAD for 20 min at room temperature. Cells were then washed in stain buffer (PBS supplemented with 2.5% FBS) and suspended in Fc Block for 5 min at RT prior to staining with a surface stain for the following antibodies: CD3 (Biolegend, #100229); CD4 (Biolegend, #100552); CD8 (Biolegend, #100714); CD44 (Biolegend, #103006); CD62L (Biolegend, #104445). After 20 min, the cells were washed with staining buffer and then fixed and permeabilized using a BD Cytoperm fixation/permeabilization solution kit according to the manufacturer's instructions. Cells were washed in perm/wash solution, followed by intracellular staining (30 min, RT) using a cocktail of the following antibodies: IFN-γ (Biolegend, #505810); IL-2 (Biolegend, #503818); IL-4 (Biolegend, #506324); TNF-α (Biolegend, #504104). Finally, the cells were washed in perm/wash solution and suspended in stain buffer. Samples were washed and acquired on an LSRFortessa (BD Biosciences). Analysis was performed using FlowJo software.

Rhesus macaque vaccination and plasma collection

For the vaccination of rhesus macaques, groups of 2∼4-year-old male rhesus macaques were immunized with LNP-circRNA^{RBD} (20 μg, n = 4; 100 μg, n = 4; 500 μg, n = 4), LNP-circRNA^{Ctrl} (circRNA without the RBD-encoding sequence; 100 μg, n = 4) or PBS (n = 4) in 300 μl (>300 μl in 500 μg dose group) via intramuscular injection in the quadriceps muscle (prime: left, boost: right) twice at a three-week interval. The plasma of immunized rhesus macaques was collected at 0, 1 and 14 days after the prime and 0, 1, 14, 28 and 35 days after post-boost.

ELISpot assay

The T cell immune responses in rhesus macaques were detected using PBMCs with commercially available Monkey IFN-γ and IL-2 ELISpot assay kits (Mabtech) and an Monkey IL-4 ELISpot assay kit (U-CyTech). The cryopreserved rhesus macaque PBMCs were thawed and cultured with prewarmed AIM-V medium. For the IFN-γ, IL-2 and IL-4 ELISpot assays, 1.0×10^5 PBMCs were stimulated with a final concentration of 1 μg/ml for each RBD peptide (Table S5). The test for each rhesus macaque was performed in two or three technical repetitions. Dimethyl sulfoxide (DMSO) served as an unstimulating control, and phytohemagglutinin (PHA-P, Sigma) and CELL STIMULATION COCKTAIL (Thermo Fisher) were used as positive controls. After 24 h of stimulation with RBD peptide pools, the streptavidin-HRP substrate (for IFN-γ and IL-2) or AEC substrate (IL-4) was added to the plate. The spots were counted by Beijing Dakewei Biotechnology Co., Ltd. The results are background (DMSO treated group) subtracted and normalized to SFC/10^6 PBMCs.

SARS-CoV-2 challenge in rhesus macaques

At 5 weeks after the boost, all the immunized rhesus macaques were challenged with 1.0×10^6 PFU of native SARS-CoV-2 virus via the intranasal (0.5 ml) and intratracheal (0.5 ml) routes. The plasma of rhesus macaques was collected, and vital clinical signs were recorded at 0, 1, 3, 5 and 7 days post virus challenge. At 7 days post virus challenge, all rhesus macaques were sacrificed to collect specimens for further experiments.

Histopathology

At 7 days after the virus challenge, the rhesus monkeys were euthanized, and necropsies were performed according to standard protocols. After dissection, a general examination of the main organs was performed. The lung tissues were harvested, fixed in 10% neutral formalin buffer and embedded in paraffin. Tissue sections (2 μm) were prepared. Slides were stained with hematoxylin and eosin (H&E). The slide images were collected by using Pannoramic DESK and analyzed with Caseviewer C. V 2.3 and Image-Pro Plus 6.0. Histopathological analysis of tissue slides was scored by 3 independent pathologists blinded to the groups of animals.

Cytokine analysis

The plasma of rhesus monkeys was isolated 24 hr post-prime or boost and diluted 5-fold or 10-fold. All plasma samples were detected using the following ELISA kits according to the manufacturer's instructions: IL-6 (Abcam, #ab242233), MCP-1 (Cloud-Clone Corp., #SEA087Si96T), TNF-α (Abcam, #ab252354), IL-1β (Cloud-clone Corp, #SEA563Si96T) and IFN-α (Chenglin, #AD0081Mk), according to the manufacturer's instructions.

QUANTIFICATION AND STATISTICAL ANALYSIS

The unpaired two-sided Student's *t* test or paired Student's *t* test was performed for comparison as indicated in the figure legends. Statistical analyses were performed with Prism 8 (GraphPad Software, Inc.).

Supplemental figures

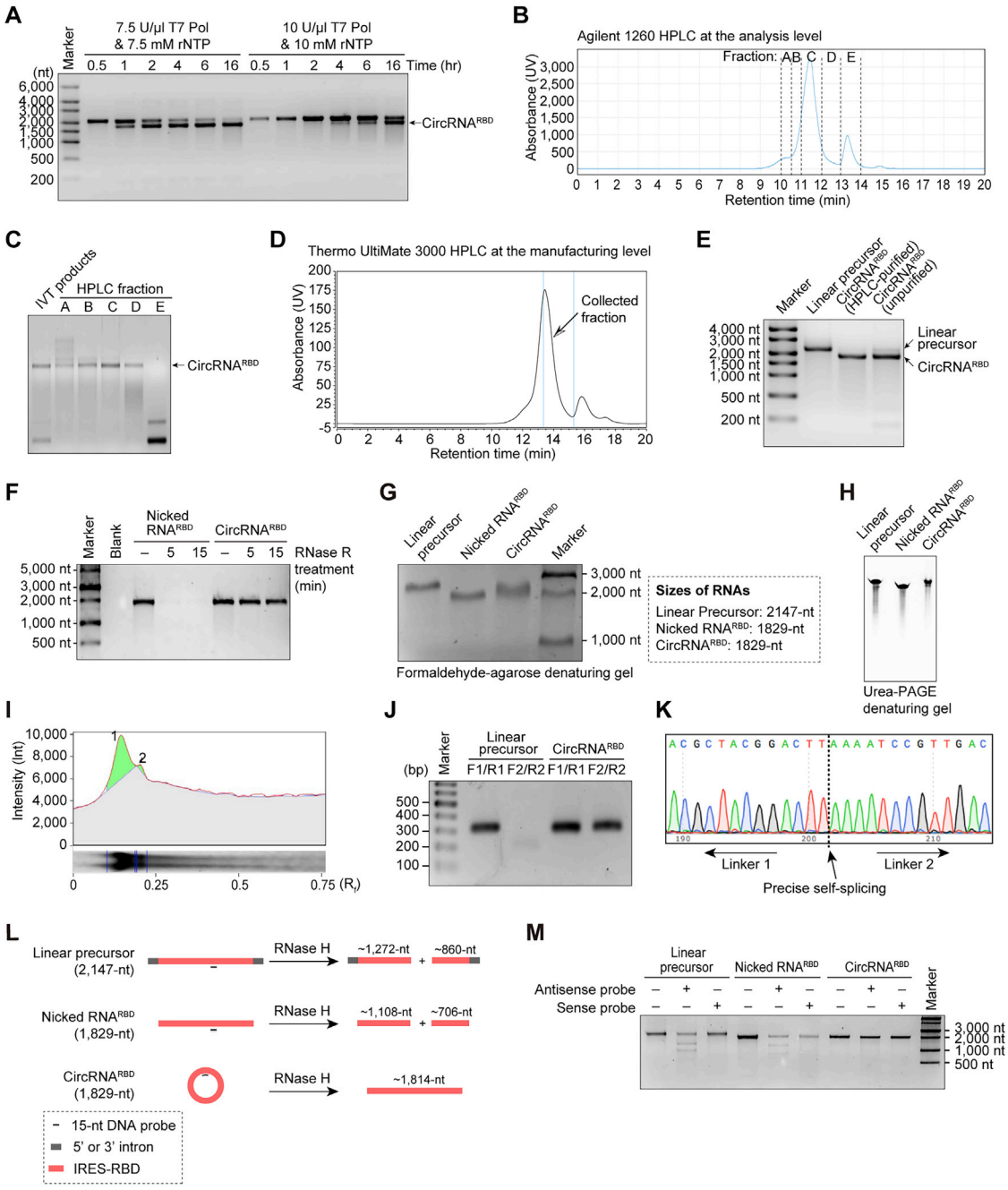

Figure S1. Optimization of the group I intron-based circRNA production approach and manufacturing of high-purity circRNAs via HPLC, related to Figure 1

(A) Agarose-gel RNA electrophoresis to test the effects of T7 RNA polymerase, rNTP, or reaction time of *in vitro* transcription on the circularization efficiency of Anabaena group I-based circRNA^{RBD} production.

(B) HPLC chromatogram of circRNA^{RBD} via an Agilent 1260 HPLC instrument.

(C) Agarose-gel RNA electrophoresis of the collected fractions in (B).

(D) HPLC chromatogram of circRNA^{RBD} via Thermo UltiMate 3000 HPLC at the manufacturing level. The latter half of the main peak was collected to produce high-purity circRNA^{RBD}.

(legend continued on next page)

(E) Agarose-gel RNA electrophoresis results for the linear RNA precursor, unpurified circRNA^{RBD}, and purified circRNA^{RBD}. The linear precursor was generated by mutating the 3′ intron of the circRNA precursor as reference band in electrophoresis.
(F) Agarose-gel electrophoresis result of nicked RNA^{RBD} and circRNA^{RBD} treated with RNase R for 5 or 15 min. Nicked RNA^{RBD} and IVT-produced linear RNAs share the same length and sequence to circRNA^{RBD}.
(G) Formaldehyde-agarose denaturing gel electrophoresis of linear precursor RNAs, nicked RNA^{RBD}, and circRNA^{RBD}. Linear precursor and nicked RNA^{RBD} served as the reference bands in electrophoresis.
(H) Urea-PAGE denaturing gel electrophoresis of linear precursor RNAs, nicked RNA^{RBD}, and circRNA^{RBD}. The time of Urea-PAGE denaturing gel electrophoresis was about 3 h, using Urea-PAGE denaturing gels (Thermo).
(I) Measurement of the purity of circRNA^{RBD} with gray scan and integral calculus analysis.
(J) Agarose-gel electrophoresis result of PCR analysis. Linear RNA precursor and circRNA^{RBD} were reverse transcribed to cDNA, followed by PCR amplification with the specific primers shown in Figure 1A.
(K) Sanger sequencing result of the PCR products in (J).
(L) Schematic diagram of RNase H assay. Linear precursor, nicked RNA^{RBD}, or circRNA^{RBD} was incubated with RNase H and a 15-nt ssDNA antisense probe (complementary to the above three kinds of RNAs) or 15-nt ssDNA sense probe (complementary to the antisense probe).
(M) Agarose-gel electrophoresis of linear precursor RNAs, nicked RNA^{RBD}, and circRNA^{RBD} after the RNase H incubation reactions.

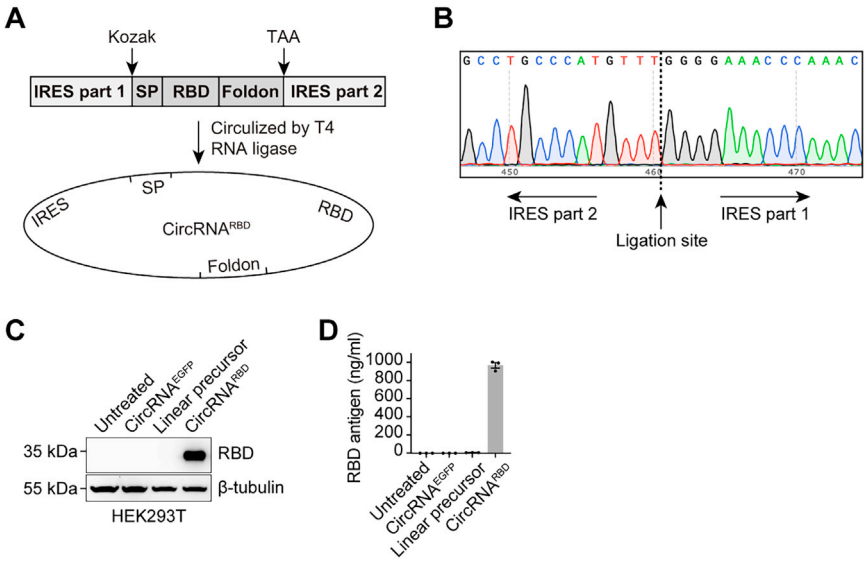

Figure S2. Expression of SARS-CoV-2 RBD antigens with circRNAs produced via T4 RNA ligase-based circularization, related to Figure 1

(A) Schematic diagram of circRNA^{RBD} circularization by T4 RNA ligase. SP, signal peptide sequence of human tPA protein. Foldon, the trimerization domain from bacteriophage T4 fibritin protein. RBD, the receptor-binding domain of the SARS-CoV-2 spike protein.

(B) Sanger sequencing result of the DNA products produced by divergent PCR.

(C) Western blot analysis showing the expression level of RBD antigens in the supernatant of HEK293T cells transfected with circRNA^{RBD} circularized by the T4 RNA ligase. The circRNA^{EGFP} and linear RNA precursor were used as controls.

(D) Quantitative ELISA measurement of the concentration of RBD antigens in the supernatant. Data are shown as the mean ± SEM (n = 3).

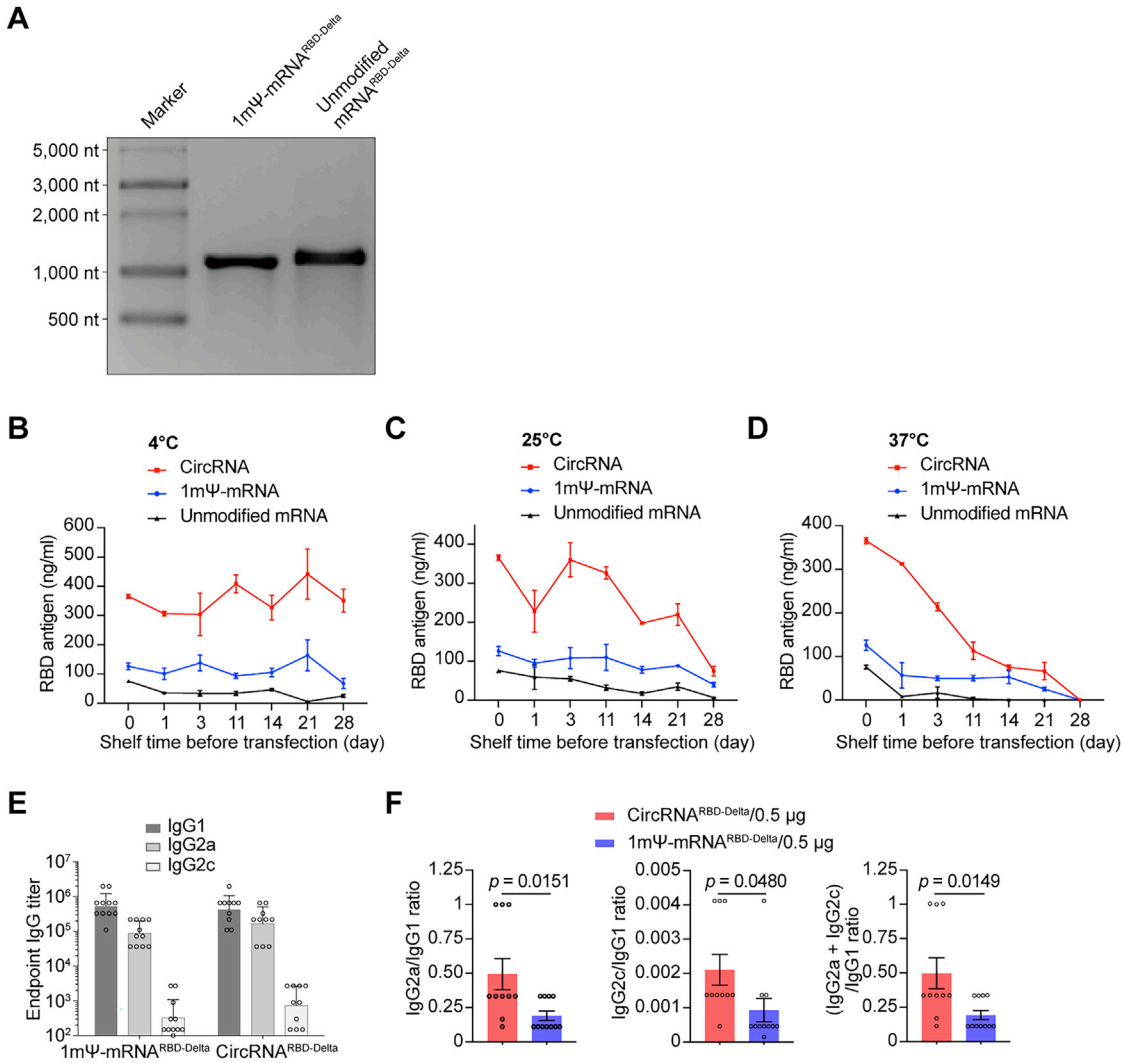

Figure S3. Measuring the expression level of RBD-Delta antigens under different storage conditions and the specific IgG2a/IgG1, IgG2c/IgG1, and (IgG2a + IgG2c)/IgG1 ratios, related to Figure 3

(A) Agarose-gel RNA electrophoresis of 1mΨ-RNA$^{RBD\text{-}Delta}$ and unmodified mRNA$^{RBD\text{-}Delta}$.

(B–D) Quantitative ELISA was used to measure the expression of RBD-Delta antigens in the supernatant of HEK293T cells transfected with LNP-circRNA$^{RBD\text{-}Delta}$, LNP-1mΨ-mRNA$^{RBD\text{-}Delta}$, and LNP-unmodified-mRNA$^{RBD\text{-}Delta}$ and stored at 4°C (B), 25°C (C), or 37°C (D). The LNP-RNAs were stored at different temperatures and transfected at different time points. Data are shown as the mean ± SEM (n = 3).

(E) Measurement of RBD-Delta-specific IgG1/IgG2a/IgG2c endpoint GMTs elicited by 0.5 μg of circRNA$^{RBD\text{-}Delta}$ vaccine or 1mΨ-mRNA$^{RBD\text{-}Delta}$ vaccine in mice. Data are shown as the geometric mean ± geometric SD (n = 10 or 11), and each symbol represents an individual mouse.

(F) Measurement of the specific IgG2a/IgG1, IgG2c/IgG1, and (IgG2a + IgG2c)/IgG1 ratios in serum from mice immunized with 0.5 μg of circRNA$^{RBD\text{-}Delta}$ or 1mΨ-mRNA$^{RBD\text{-}Delta}$. Data are shown as the mean ± SEM (n = 10 or 11), and each symbol represents an individual mouse. Unpaired two-sided Student's t test was performed for comparison, as indicated in the figures.

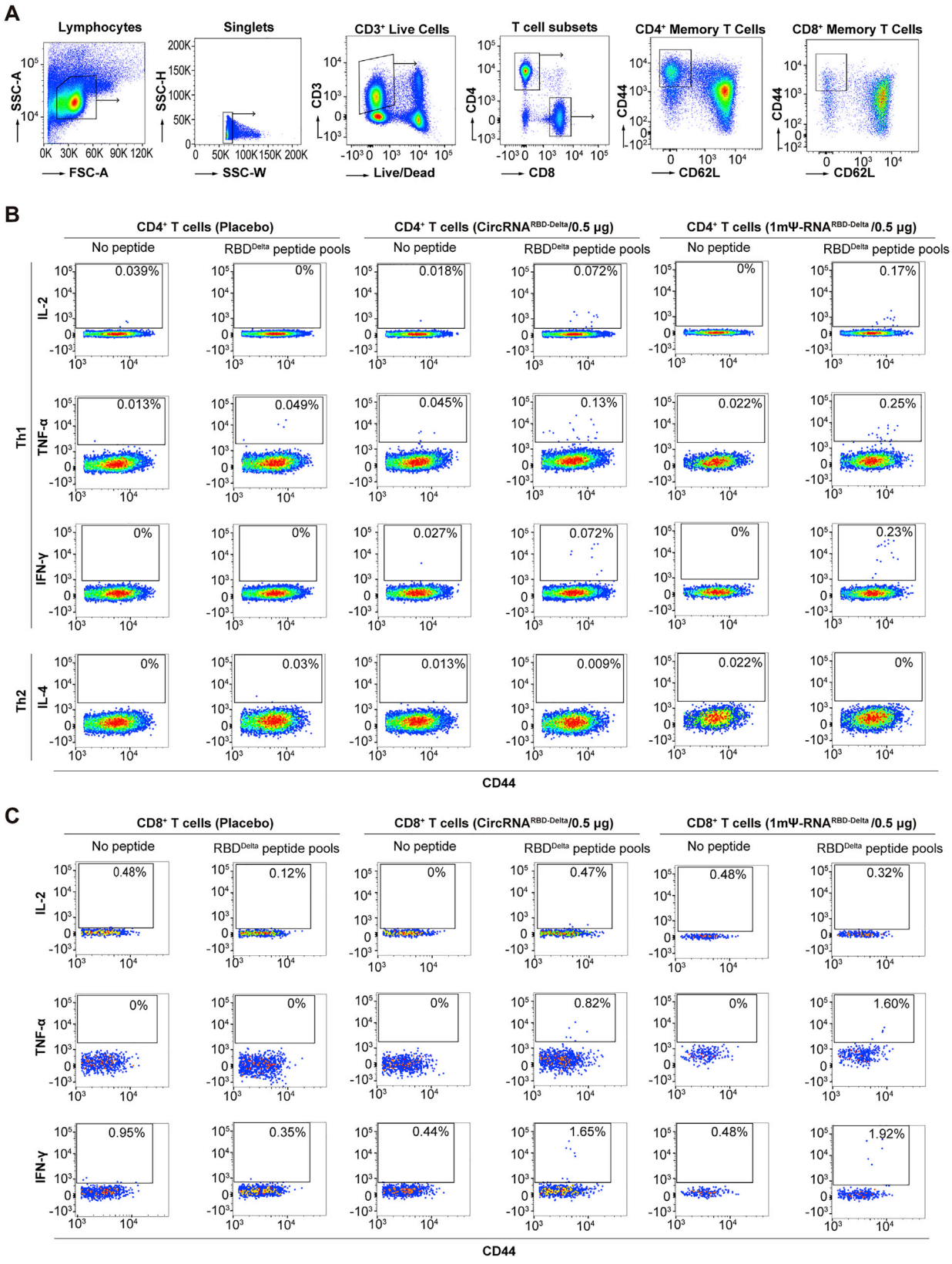

(legend on next page)

Figure S4. Flow panel and gating strategy to quantify SARS-CoV-2-RBD-specific T cells in mice, related to Figure 4

(A) The plots show the gating strategy of single and viable T cells in splenocytes. $CD4^+$ or $CD8^+$ Tem cells ($CD44^+CD62L^-$) were further analyzed to detect the expression of cytokines stimulated by corresponding RBD-Delta peptide pools.

(B and C) Represented unvaccinated and vaccinated cohorts are shown for specific $CD4^+$ T cell responses (B) and $CD8^+$ T cell responses (C).

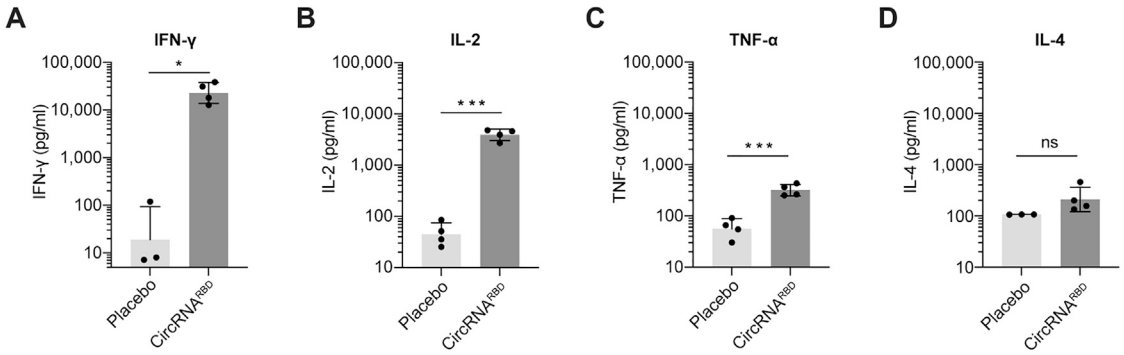

Figure S5. The ELISA results showing the cytokine levels in the supernatants of peptide pool-stimulated splenocytes, related to Figure 4

(A–D) Measurement of the level of IFN-γ (A), IL-2 (B), TNF-α (C), or IL-4 (D) in the supernatants of peptide pool-stimulated splenocytes with ELISA. The data are shown as the geometric mean ± geometric SD (n = 3 or 4), and each symbol represents an individual mouse. Unpaired two-sided Student's t test was performed for the comparison, as indicated in the figures; *p < 0.05; **p < 0.01; ***p < 0.001; ****p < 0.0001; ns, not significant.

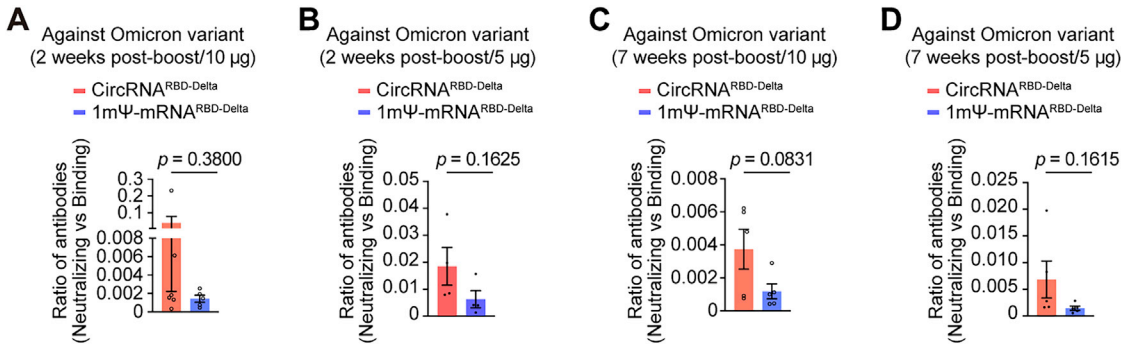

Figure S6. The circRNA$^{RBD\text{-}Delta}$ vaccine elicited a high level of neutralizing antibodies against the Omicron variant, related to Figure 5

(A and B) Measurement of the ratio of (neutralizing antibodies)/(binding antibodies) elicited by 10 μg (A) or 5 μg (B) of circRNA$^{RBD\text{-}Delta}$ vaccine or 1mΨ-mRNA$^{RBD\text{-}Delta}$ vaccine in sera collected 2 weeks after the boost. The ratio of (NT50)/(endpoint GMT) of each mouse was calculated.

(C and D) Measurement of the ratio of (neutralizing antibodies)/(binding antibodies) elicited by 10 μg (C) or 5 μg (D) of circRNA$^{RBD\text{-}Delta}$ vaccine or 1mΨ-mRNA$^{RBD\text{-}Delta}$ vaccine with the sera collected 7 weeks after the boost. The ratio of (NT50)/(endpoint GMT) of each mouse was calculated.

In (A)–(D), data are presented as the mean ± SEM (n = 4–6), and each symbol represents an individual mouse. The unpaired two-sided Student's t test was performed for comparison, as indicated in the figures.

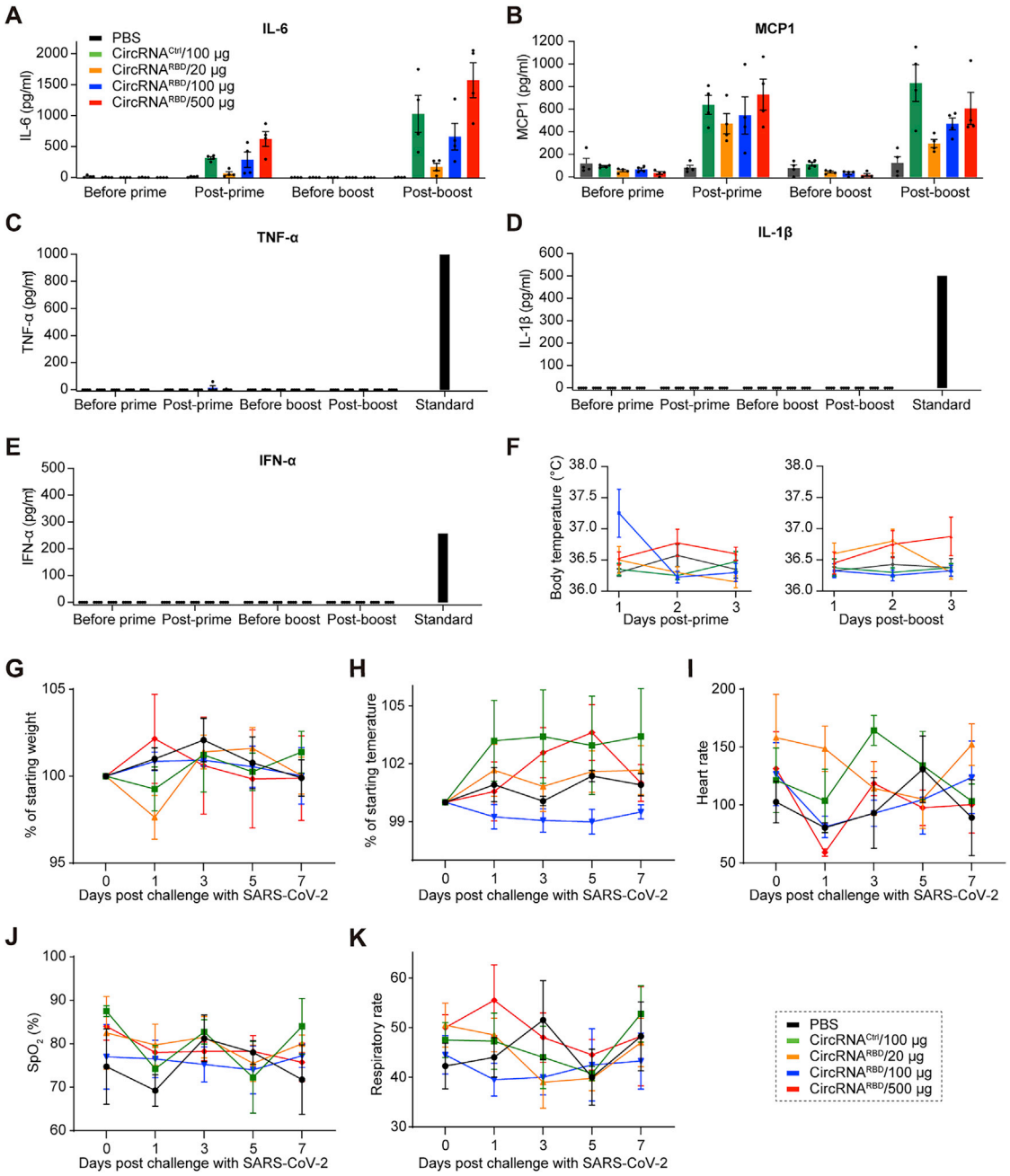

Figure S7. CircRNA vaccine caused no obvious clinical signs of illness in rhesus macaques, related to Figure 6

(A–E) Measurement of the IL-6 (A), MCP-1 (B), TNF-α (C), IL-1β (D), and IFN-α (E) level in the plasma of immunized rhesus macaques.

(F) Monitoring the body temperature of rhesus macaques. Body temperature was monitored within 3 days after the prime and boost doses. In (A)–(F), data are shown as the mean ± SEM (n = 4).

(G–K) The body weight (G), temperature (H), heart rate (I), oxygen saturation (J), and respiratory rate (K) were monitored after challenge with SARS-CoV-2. Data are shown as the mean ± SEM (n = 4).